

# Standard Model Higgs Boson Searches through the 125 GeV Boson Discovery

Gregorio Bernardi<sup>1</sup> and Matthew Herndon<sup>2</sup>

<sup>1</sup>*LPNHE, Universités Paris VI & VII, CNRS/IN2P3, Paris, France*

<sup>2</sup>*University of Wisconsin, Madison, Wisconsin 53706-1390, USA*

Searches for the standard model Higgs boson are reviewed from the 2 TeV run of the Tevatron with  $\simeq 10 \text{ fb}^{-1}$  of recorded data, and from the 7 and 8 TeV runs of the LHC, with  $\simeq 5$  and  $\simeq 6 \text{ fb}^{-1}$ , respectively, i.e., until the July-2012 discovery of a new particle by the LHC experiments. The CMS and ATLAS Collaborations observe independently a new boson with mass  $\simeq 125 \text{ GeV}$ , mainly through its bosonic decays in  $\gamma\gamma$ ,  $ZZ$ , and  $W^+W^-$ , consistent with the standard model Higgs boson. The CDF and D0 experiments combine their results to see evidence of a similar particle produced in association with a vector boson and decaying fermionically in  $b\bar{b}$ .

PACS numbers: 13.85.Rm, 14.80.Bn

<b>Contents</b>			
<b>I. Introduction</b>	2	B. $WH \rightarrow l\nu b\bar{b}$	12
<b>II. SM Higgs boson phenomenology and search strategies</b>	2	C. $ZH \rightarrow llb\bar{b}$	12
A. Phenomenology of SM Higgs Boson production	2	D. $ZH \rightarrow \nu\nu b\bar{b}$ and $VH \rightarrow \cancel{E}_T b\bar{b}$	13
B. Phenomenology of SM Higgs boson decay	3	E. CDF and D0 results on $H \rightarrow b\bar{b}$ searches	14
C. Standard model fits	3	F. Searches in $\tau_h$ final states	14
D. Direct constraints from LEP	3	G. Searches in $H \rightarrow \gamma\gamma$	14
E. Search strategies at the Tevatron	4	H. Searches for $t\bar{t}H$ production	14
F. Search strategies at the LHC	4	<b>VI. Tevatron high mass Higgs boson searches</b>	15
G. Simulation of background and signal processes	5	A. Diboson analysis: $WW$ , $WZ$ and $ZZ$	15
<b>III. The Tevatron and the CDF and D0 detectors</b>	5	B. Analysis Topologies	15
A. Tracking detectors	5	C. CDF and D0 results at high Higgs boson mass	16
B. Calorimeters	6	<b>VII. LHC searches in bosonic Higgs boson decays</b>	16
C. Muon detectors	6	A. LHC diboson physics	16
D. Triggering systems	6	B. Searches in $H \rightarrow \gamma\gamma$	17
E. Physics object identification at the Tevatron	6	C. Searches in $H \rightarrow ZZ \rightarrow \ell^+\ell^-\ell^+\ell^-$	18
1. Lepton identification	6	D. Searches in $H \rightarrow W^+W^- \rightarrow \ell^+\nu\ell^-\bar{\nu}$	19
2. Jets, $b$ jets, and missing transverse energy	7	E. Searches in $H \rightarrow WW, ZZ$ with decays of one boson to quarks or neutrinos	20
<b>IV. The LHC, ATLAS, and CMS experiments</b>	7	<b>VIII. LHC searches in fermionic Higgs boson decays</b>	21
A. Tracking detectors	8	A. Searches in $H \rightarrow \tau^+\tau^-$	21
B. Calorimeters	8	B. Searches in $H \rightarrow b\bar{b}$	22
C. Muon systems	9	C. Searches for $t\bar{t}H$ production	22
D. Triggering	9	<b>IX. ATLAS, CMS, and Tevatron Results</b>	22
E. Physics object identification at the LHC	9	A. Limits and combination methods	22
1. Charged lepton identification	9	B. ATLAS and CMS results	23
2. Photon identification	10	C. Tevatron combined results	27
3. Light and heavy flavor jets	10	D. Conclusion and prospects	29
4. Missing transverse energy	10	<b>References</b>	30
5. Particle flow	11		
<b>V. Tevatron low-mass Higgs boson searches</b>	11		
A. $VZ$ with $Z \rightarrow b\bar{b}$ as a test of the $VH$ search	11		

## I. INTRODUCTION

The origin of the masses of elementary particles, one of the remaining puzzles of the highly successful theoretical model of the standard model (SM), has a potential solution requiring the existence of only one doublet of complex scalar fields. Then the finite mass of the SM elementary fermions and bosons can be explained, after spontaneous electroweak symmetry breaking (EWSB) of the originally massless Lagrangian [1–7]. This minimal approach could be confirmed if the remnant of such a breaking, the Higgs boson, is observed with the couplings and properties predicted in the SM. The SM Higgs boson does not solve all problems related to the EWSB, and is maybe only one component of the fields involved. However, its discovery would be a major step in the final validation of the SM in that it would show a unified approach to the generation of boson and fermion masses. While there are other approaches to explain EWSB, none is so far as successful as the Higgs mechanism, so we concentrate in this review on the experimental searches for such a boson. With the recent observation of a new boson at the LHC, a major step forward has been accomplished, but a complete validation has yet to be done. The data taking has been concluded at the Tevatron and at the LHC for the center of mass energy of 7 TeV, while the data are still being accumulated at 8 TeV. However, given the crucial discovery made using these searches, we provide a dedicated review based on the publications which immediately followed the discovery and on the results available at that time, without extending the results reviewed beyond discovery time.

To review these milestone results, we first briefly explain the phenomenology of the production and decay of the SM Higgs boson, the indirect and direct constraints on the SM Higgs from other measurements, and the search strategies at hadron colliders, first pioneered at the Tevatron and then extended at the LHC. We review the Tevatron experiments, and their low-mass and high-mass analyses, then the LHC experiments, and their searches in bosonic and fermionic Higgs boson decays. Finally we review the combinations of these searches, which led to the discovery of a new boson by ATLAS and CMS independently, and to the evidence, from the Tevatron, for a particle consistent with this new boson. We conclude by briefly discussing the current knowledge on this new boson and on short term prospects.

## II. SM HIGGS BOSON PHENOMENOLOGY AND SEARCH STRATEGIES

### A. Phenomenology of SM Higgs Boson production

The SM Higgs boson is a  $CP$ -even scalar, and its couplings to fermions and to gauge bosons are proportional to the fermion masses, and to the squares of the boson masses, respectively. The effective Higgs boson-gluon

coupling  $Hgg$  is dominated at leading order (LO) by a one-loop graph in which the  $H$  couples dominantly to a virtual  $t\bar{t}$  pair. The much weaker effective coupling to photons  $H\gamma\gamma$  proceeds also at LO via a loop, dominated by a virtual  $W^+W^-$  pair [8]. The dominant cross section for Higgs boson production is the  $gg \rightarrow H$  ( $ggH$ ) process, which is known at next-to-next-to-leading order (NNLO) from perturbative calculation in quantum chromodynamics (QCD). This calculation is performed using a large top-mass limit approximation and a similar calculation at next-to-leading order (NLO) in QCD has been performed for arbitrary top mass [9–13]. The NLO QCD corrections approximately double the leading-order prediction, and the NNLO corrections add approximately 50% to the NLO prediction. NLO electroweak corrections range between 0% and 6% of the LO term [14–16]. Mixed QCD-electroweak corrections  $O(\alpha\alpha_s)$  are also included [17]. Soft-gluon contributions to the cross sections have been resummed at next-to-leading logarithmic (NLL), next-to-next-to-leading logarithmic (NNLL) and partial next-to-next-to-next-to-leading logarithmic (NNNLL) accuracy [18–27]. Predictions for the gluon fusion cross sections at NNLO or through soft-gluon resummation up to NNLL accuracy and two-loop electroweak effects can be found in Ref. [17, 27–29], including differential cross section as a function of Higgs boson transverse momentum [30, 31]. Uncertainties are dominated by the modeling of parton distribution functions (PDFs) and choices of fragmentation and renormalization scales and are  $\simeq 25\%$  at the Tevatron and  $\simeq 15\%$  at the LHC. The cross sections have also been computed exclusively for Higgs boson production in association with one jet [32, 33] and in association with two jets [34][35].

At the Tevatron, the next most important production processes are Higgs boson production in association with vector bosons ( $VH$ ), where  $V$  is a massive  $W$  or  $Z$  vector boson. The cross sections for  $q\bar{q} \rightarrow WH$  or  $ZH$  are

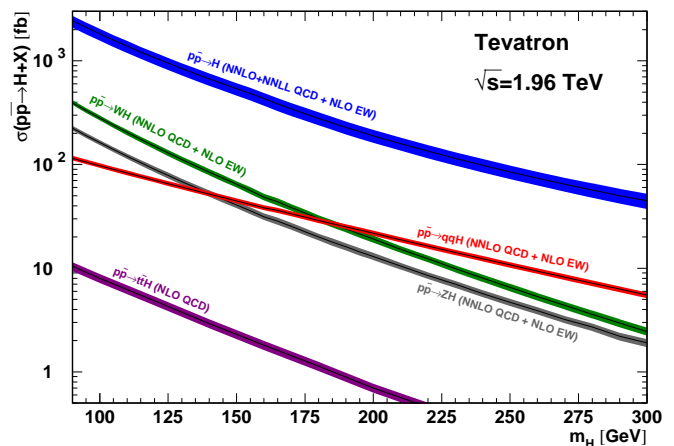


FIG. 1: SM Higgs boson production cross sections for  $p\bar{p}$  collisions at 1.96 TeV [9–13, 37–49, 51–54] as functions of its mass.

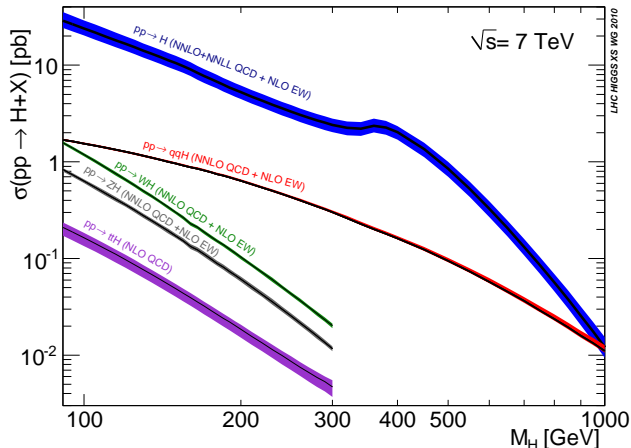


FIG. 2: SM Higgs boson production cross sections for  $pp$  collisions at 7 TeV [55], as functions of its mass.

known at NNLO for the QCD corrections and at NLO for the electroweak corrections [36–42], with a total uncertainty of  $\simeq 5\%$ . For the vector boson fusion (VBF) process  $qq \rightarrow qqH$ , which dominates over the associated production at the LHC, the production cross sections are known at NNLO in QCD and at NLO for the electroweak corrections, with a total theoretical uncertainty  $\simeq 5\%$  [43–49], which becomes larger when exclusive requirements are put on the jets [50]. For the associated production process  $t\bar{t}H$ , the cross section has been calculated at NLO in QCD [51–54].

The cross sections for the production of SM Higgs bosons are summarized in Fig. 1 for  $p\bar{p}$  collisions at the Tevatron, and in Fig. 2 for  $pp$  collisions at the LHC at  $\sqrt{s} = 7$  TeV [55, 56]. Cross sections at  $\sqrt{s} = 8$  TeV have a similar behavior but are 20–30% larger at low Higgs boson mass ( $m_H < 135$  GeV).

### B. Phenomenology of SM Higgs boson decay

The branching ratios for the most relevant decay modes of the SM Higgs boson are shown in Fig. 3 as functions of  $m_H$ . For masses below 135 GeV, decays to fermion pairs dominate, of which the decay  $H \rightarrow b\bar{b}$  has the largest branching ratio. For these lower masses, the total decay width is less than 10 MeV. For Higgs boson masses above 135 GeV, the  $WW$  decay dominates with an important contribution from  $H \rightarrow ZZ$  above threshold. The decay width rises rapidly, reaching about 1 GeV at  $m_H = 200$  GeV and 100 GeV at  $m_H = 500$  GeV. Above the  $t\bar{t}$  threshold, the branching ratio into top-quark pairs increases rapidly as a function of the Higgs boson mass, reaching a maximum of about 20% at  $m_H \simeq 450$  GeV.

### C. Standard model fits

While the mass of the SM Higgs boson is not given by the theory, indirect constraints for the SM Higgs boson mass can be derived from fits to precision measurements of electroweak observables. The Higgs boson contributes to the observed  $W$  and  $Z$  masses through loop effects, leading to a logarithmic sensitivity of the ratio of the  $W$  and  $Z$  gauge boson masses on the Higgs boson mass. The top quark contributes to the observed  $W$  boson mass through loop effects that depend quadratically on the top mass, which thus also plays an important role in the global fit. A global fit to precision electroweak data, accumulated over the last two decades mainly at LEP, SLC and the Tevatron, gives  $m_H = 94_{-24}^{+29}$  GeV or  $m_H < 152$  GeV at 95% C.L. [57, 58]. Measurements of the top-quark mass [ $173.2 \pm 0.9$  GeV ([59])] and of the  $W$  boson mass [ $80.385 \pm 0.015$  GeV ([60])] were used for these constraints. These results, compared to the allowed direct search range from March 2012 are shown in Fig. 4.

### D. Direct constraints from LEP

At the LEP  $e^+e^-$  collider, which operated between 1989 and 2000 at  $\sqrt{s} = 90$  GeV (LEP1) or 160–209 GeV (LEP2), the SM Higgs boson is generally produced through Higgsstrahlung in the  $s$  channel,  $e^+e^- \rightarrow HZ$  [61, 62], where the  $Z$  boson in the final state is either virtual (LEP1) or on shell (LEP2). The SM Higgs boson can also be produced by  $WW$  and  $ZZ$  fusion in the  $t$  channel [63–65], but at LEP these processes have small cross sections. The sensitivity of the LEP searches to the Higgs boson strongly depends on the center of mass energy  $E_{\text{cm}}$ . For  $m_H < E_{\text{cm}} - m_Z$ , the cross section is of the order of 1 pb or more, while for  $m_H > E_{\text{cm}} - m_Z$ , the cross section is smaller by at least an order of magnitude.

Each production and decay mode was analyzed sepa-

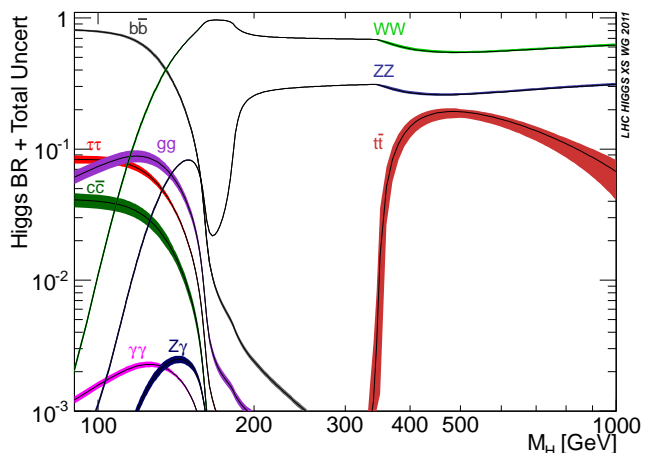


FIG. 3: Branching ratios for the main decays of the SM Higgs boson as functions of its mass

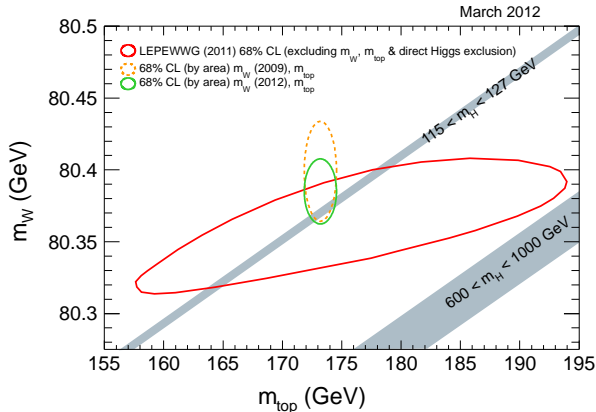


FIG. 4: Constraints from the top-quark mass, the  $W$  boson mass and other SM measurements compared to the allowed Higgs search range in March 2012.

rately. Data recorded at each center of mass energy were studied independently and the results from the four LEP experiments were then combined. Strong upper bounds on the  $e^+e^- \rightarrow ZH$  cross section are obtained for Higgs boson masses between 1 keV and  $\simeq 115$  GeV. The combination of the LEP data yields a 95% C.L. lower bound of 114.4 GeV for the mass of the SM Higgs boson [66]. The median limit expected in a large ensemble of identical experiments when no signal is present (simply called “expected limit” in the following) is 115.3 GeV and was limited by the collision energy achieved by the accelerator.

### E. Search strategies at the Tevatron

At the Tevatron, the delivered luminosity and the Higgs boson production cross section are sufficient to be sensitive at the 95% C.L. to a Higgs boson having a mass between 90 and 185 GeV, i.e., significant overlap with the LEP excluded region at lower masses, and with the LHC. Sensitivity is strongest at lower mass, 90-120 GeV and around the  $H \rightarrow WW$  threshold ( $\simeq 145 - 185$  GeV) where the best expected sensitivity reaches approximately 4 standard deviations. The search strategy gives priority to direct production and the  $H \rightarrow WW$  decay mode at high mass, which allowed in 2009 for the extension of the experimental limits on the SM Higgs boson mass beyond the LEP exclusion limit for the first time after almost ten years [67], with subsequent enlarged excluded regions [68, 69]. These results in combination with the precision electroweak measurements showed, before the LHC produced significant results, that a mass of the SM Higgs boson above  $\simeq 145$  GeV was excluded at 95% C.L. [70]

At low-mass, the associated production channels ( $WH, ZH$ ) involving  $H \rightarrow b\bar{b}$  are the most sensitive, with a significant additional contribution from direct production with  $H \rightarrow WW$  decay at Higgs boson masses as low as 120 GeV. The  $WH$  and  $ZH$  channels with  $H \rightarrow b\bar{b}$  are

particularly important since this decay mode will probably not be observed at the  $5\sigma$  level at ATLAS or CMS before additional statistics has been accumulated after the upgrade to the full energy foreseen for 2015. Even though it will be measured more precisely in the LHC experiments than at the Tevatron, once the full 2011-2012 statistics will have been analyzed, the contribution of the Tevatron results will still be significant.

### F. Search strategies at the LHC

The LHC was designed to have a full reach to discover the Higgs boson, from 0.1 to 1 TeV, which is the region where it was theoretically expected to be. The high energy of the LHC proton-proton collider substantially increases the cross section for production of a Higgs boson via gluon fusion ( $ggH$ ). The cross section for vector boson fusion and associated production are also enhanced. Because of a more unfavorable signal-to-background ratio in associated production (due to the initial dominant  $qg$  or  $gg$  vs  $q\bar{q}$  hard interaction), the search strategy gives priority to inclusive production and the  $H \rightarrow \gamma\gamma$  or  $H \rightarrow ZZ$  decay modes at lower masses, or simply to the  $H \rightarrow ZZ$  decay mode at higher masses. Both modes allow possible discovery as soon as the available integrated luminosity is sufficient (of the order of  $10 \text{ fb}^{-1}$ ). Also at high mass  $ZZ$  and  $W^+W^-$  Higgs boson decay modes with  $W$  and  $Z$  decays to jets or  $Z$  decays to neutrinos have strong sensitivity. The  $H \rightarrow WW$  channel is best searched in the region around the  $WW$  on-shell decay threshold, but does not have the mass resolution to observe a clear resonance signal. No single channel dominates the sensitivity, so the search is also performed through combination of all channels. Already as of 2011 this strategy has allowed for the exclusion of a Higgs boson between masses of approximately 130 to 500 GeV.

In addition, once a new particle is observed all channels are crucial to understanding its nature. In particular the fermionic decays (in pairs of  $\tau$  leptons or  $b$  quarks) are a major source of information on fermion couplings, but may require a higher luminosity. In both channels it is possible to find evidence for fermionic decays and measure Yukawa couplings of the Higgs boson to the fermions given SM couplings using data collected before the upgrade to the full energy foreseen for 2015. The  $\tau$  mode is the stronger channel since it can be seen in all Higgs boson production mechanisms with manageable signal to background. Other fermionic decays will not be not observable before a significant luminosity upgrade not foreseen before several years, assuming SM branching ratios, although information is gained about the Higgs boson coupling to the top quark through the loop production diagrams.

### G. Simulation of background and signal processes

The general strategies used to generate background and signal processes at both the Tevatron and LHC are summarized in this section.

i) High cross section backgrounds  $W/Z + \text{jets}$ : the SM background processes  $Wq\bar{q} \rightarrow \ell\nu q\bar{q}$  or  $Zq\bar{q} \rightarrow \ell^+\ell^-q\bar{q}$ , where  $q$  is used to represent light partons  $u, d, s$  and gluons ( $g$ ), and higher cross section diboson processes, are simulated using Monte Carlo (MC) matrix element event generators such as ALPGEN[71], MADGRAPH[72], and POWHEG[73–75]. Separate samples are generated for light parton multiplicities and in each case samples are generated for each of the final state decay lepton flavors  $\ell = e, \mu, \tau$ . To account for the subsequent hadronization and development of partonic showers, the matrix event generators are interfaced to PYTHIA[76] using the M.L. Mangano (MLM) factorization (“matching”) scheme [71] to remove events where soft jets developed in partonic showering overlap phase space already covered by the matrix event generator.

ii) top-antitop, “single” top and diboson production:  $t\bar{t}$  production has been studied since the Tevatron run 1 and is now also studied at the LHC. The electroweak production of (single) top-quark has been observed at the Tevatron by the CDF and D0 collaboration in 2008 [77, 78] and also more recently by the LHC experiments. Similarly diboson production ( $WW, WZ, ZZ$ ) has been measured at the Tevatron and LHC. Extensive studies of top, single top, and diboson production have been performed by the collaborations showing that the normalization and kinematic distributions of these processes are well modeled by a variety of programs including CompHep[79, 80], MC@NLO[81], MADGRAPH, and POWHEG interfaced to PYTHIA. The diboson processes  $WW$  and  $ZZ$  also have substantial contributions from gluon-gluon initial states which are generated using the specialized generators GG2WW[82] and GG2ZZ[83] at LHC experiments. In cases where there are multiple additional partons in the final state, the data are not as constraining and the techniques listed in section i) are applied.

iii) backgrounds with  $b$ -flavored quarks,  $Wb\bar{b}, Zb\bar{b}$ : These production processes are generated using similar techniques to those described above. Normalization k-factors measured in data are applied to these associated vector boson with  $b$ -flavored quark production processes, as their total cross sections are not precisely predicted. Scale factors to account for efficiency differences in simulation and data for  $b$ -jet identification are applied, as is also the case for other processes with  $b$ -jet in the final state.

iv) Higgs boson signal samples: these are generated using programs such as PYTHIA and POWHEG interfaced to PYTHIA. In the case of gluon fusion production the kinematics calculated at NNLO can differ from leading order generation and samples are re-weighted to differential NNLO calculations.

For each background or signal the total cross section

is normalized to the best available NLO or NNLO calculations.

### III. THE TEVATRON AND THE CDF AND D0 DETECTORS

The Tevatron was a proton-antiproton collider which completed operation in September 2011. The Higgs boson searches took place during run II (2002-2011) in which it was configured to collide beams of 36 bunches with 1.96 TeV center of mass energy and provided an integrated dataset of  $10 \text{ fb}^{-1}$  to the CDF and D0 experiments (note integrated luminosities given in this review refer to integrated luminosity delivered with the detectors in an operational condition sufficient to be used in physics analysis). The instantaneous luminosity reached  $4 \times 10^{32} \text{ cm}^2 \text{ s}^{-1}$ , but the effect of the overlay of multiple interactions remained manageable.

The main components of the run II CDF and D0 detectors are the tracking detectors, calorimeters and muon detectors. Specific details of the CDF and D0 detector subsystems are available in [84] and [85], respectively, while here we briefly summarize their main characteristics. The kinematic properties of particles and jets are defined with respect to the origin of the detector coordinate system which is at the center of the detector. To quantify polar angles the pseudorapidity variable, defined as  $\eta = -\ln \tan(\theta/2)$ , is used where  $\theta$  is the polar angle in the corresponding spherical polar coordinate system.

#### A. Tracking detectors

The CDF tracking system consists of an eight layer silicon micro-strip tracker and an open-cell drift chamber referred to as the central outer tracker (COT), both immersed in a 1.4 T solenoidal magnetic field. These systems combined provide charged particle tracking and precision vertex reconstruction in the pseudorapidity region  $|\eta| < 1.0$  with partial coverage in the COT to  $|\eta| < 1.7$  while the two outer layers of the silicon detector extend the tracking capability to  $|\eta| < 2.0$ .

The D0 tracking system is located immediately surrounding the interaction point and consists of an inner silicon micro-strip tracker (SMT) surrounded by an outer central scintillating fiber tracker (CFT). Both the SMT and CFT are situated within a 2 T magnetic field provided by a solenoidal magnet surrounding the entire tracking system. The SMT is used for tracking up to  $|\eta| < 2.5$  and for vertex reconstruction. The central fiber tracker is also used for tracking and vertex reconstruction, and provides precise tracking coverage up to  $|\eta| < 1.7$ .

## B. Calorimeters

The CDF calorimeter systems are used to measure the energy of charged and neutral particles produced in  $p\bar{p}$  collisions and are arranged around the outer edges of the central tracking volume and solenoid. These systems consist of modular sampling scintillator calorimeters with a tower based projective geometry. The inner electromagnetic sections of each tower consist of lead sheets interspersed with scintillator, and the outer hadronic sections are composed of scintillator sandwiched between sheets of steel. The CDF calorimeter consists of two sections: a central barrel calorimeter and forward end plug calorimeters covering the pseudorapidity region  $|\eta| < 3.64$ . The calorimeters can identify and measure photons, jets from partons, missing transverse energy, and in combination with information from other systems electron and tau leptons.

The D0 liquid-argon calorimeter system is used for the identification and energy measurement of electrons, photons, and jets, and also allows the measurement of the missing transverse energy ( $\cancel{E}_T$ ) of the events, typically from unobserved neutrinos. The central calorimeter (CC) covers detector pseudorapidities  $|\eta| \leq 1.1$  and the two additional end-cap calorimeters extend the range up to  $|\eta| = 4.2$ . They are located outside of the tracking and solenoid systems. The calorimeters are subdivided into electromagnetic (EM) followed by fine hadronic and then coarse hadronic sections. The intercryostat plastic scintillator detectors complete the calorimeter coverage in the intermediate pseudorapidity region  $0.8 < |\eta| < 1.4$ .

## C. Muon detectors

The CDF muon detector is made up of four independent detector systems outside the calorimeter modules and consists of drift chambers interspersed with steel layers to absorb hadrons. The central muon detector (CMU) is mounted directly around the outer edge of the central calorimeter module and detects muons in the pseudorapidity region  $|\eta| < 0.6$ . The central muon extension is composed of spherical sections and extends the pseudorapidity coverage in the range  $0.6 < |\eta| < 1.0$ . The central muon upgrade (CMP) surrounds portions of the CMU and central muon extension (CMX) systems covering gaps in angular coverage and allowing excellent identification of higher momentum muons due to additional layers of steel absorber. The barrel muon upgrade (BMU) is a barrel shaped extension of the muon system in the pseudorapidity region  $1.0 < |\eta| < 1.5$ . The CMX, CMP and BMU systems also include matching scintillator systems which provide timing information to help identify collision produced muons.

The D0 muon detector system consists of a central muon detector system covering the range  $|\eta| < 1$  and a forward muon system which covers the region  $1 < |\eta| < 2$ . Scintillation counters are included for triggering purposes

and a 1.8 T toroidal iron magnet makes it possible to determine muon momenta and perform tracking measurements within the muon system alone, although in general the central tracking information is also used for muon reconstruction.

## D. Triggering systems

The CDF trigger system consists of three levels. Level one trigger hardware consists of dedicated electronics that operate at the beam crossing frequency. The level one trigger can identify and measure the transverse momentum of charged particles using COT information and be combined with information from the calorimeters or muon systems to provide a trigger for leptons. The calorimeter trigger hardware measures energy clusters which are used to identify jets and photons as well as an imbalance in event transverse energy interpreted as  $\cancel{E}_T$ . The second level trigger hardware at CDF refines the measurements of the level one trigger at higher precision. The level two trigger can also include tracking and vertexing information from the silicon detectors. The third level of the trigger operates on commercial computers (PCs) and executes fast versions of the full offline reconstruction software.

The D0 trigger system also has three trigger levels referred to as L1, L2 and L3. Each consecutive level receives a lower rate of events for further examination. The L1 hardware based elements of the triggers used in the electron channel typically require calorimeter energy signatures consistent with an electron. This is expanded at L2 and L3 to include trigger algorithms requiring an electromagnetic object together with at least one jet for which the L1 requirement is calorimeter energy depositions consistent with high- $p_T$  jets. For muon samples, events are triggered using the logical .OR. of the full list of available triggers of the D0 experiment. The muon trigger pseudorapidity coverage is restricted to  $|\eta| < 1.6$  where the majority of the  $W$ +jet events ( $\simeq 65\%$ ) are collected by triggers requiring high- $p_T$  muons at L1. Events not selected by the high- $p_T$  muon triggers are primarily collected by jet triggers.

## E. Physics object identification at the Tevatron

### 1. Lepton identification

Isolated electrons are reconstructed in the calorimeter and are selected in the pseudorapidity regions  $|\eta| < 2.8$  at CDF, and at  $|\eta| < 1.1$  and  $1.5 < |\eta| < 2.5$  at D0. The EM showers are required to pass spatial distribution requirements consistent with those expected from electrons for each section of the calorimeter. In the D0 CC region, a reconstructed track, isolated from other tracks, is also required to be matched to the EM shower while in CDF

a matching track is required within the coverage of the COT tracker.

Muons are selected by requiring a local track spanning all layers of the muon detector system (for D0 both within as well as outside of the toroidal magnet). A spatial match is then required to a corresponding track in the COT (CDF) or CFT (D0). To suppress muon background events originating from the semileptonic decay of hadrons, muon candidate tracks are required to be separated from jets by at least  $\Delta R = \sqrt{(\Delta\eta)^2 + (\Delta\phi)^2} > 0.5$ . A veto against cosmic ray muons is also applied using scintillator timing information in D0 and a specialized tracking algorithm is used at CDF to track cosmic ray muons passing through both sides of the detector. Muons can also be identified as a minimum ionizing isolated track in CDF for regions without muon coverage taking advantage of the fact that muons interact with low probability in the material of the calorimeter leaving only a small ionization signature.

Multivariate algorithms (MVA) [86] are used to enhance efficiency and background rejection in some electron and muon based analysis.

Tau lepton decays into hadrons are characterized as narrow, isolated jets with lower track multiplicities than jets originating from quarks and gluons. Three types of tau lepton decays are distinguished by their detector signature. One-track tau decays consisting of energy deposited in the hadronic calorimeter associated with a single track are denoted as tau-type 1; tau-type 2 corresponds to one-track tau decays with energy deposited in both the hadronic and EM calorimeters, associated with a single track; and tau-type 3 are multitrack decays with energy in the calorimeter and two or more associated tracks with invariant mass below 1.7 GeV. In D0, a set of neural networks, one for each tau type, is applied to discriminate hadronic tau decays from jets. The input variables are related to isolation and shower shapes, and exploit correlations between calorimeter energy deposits and tracks. When requiring the neural network discriminants to be above thresholds optimized for each tau type separately, typically 65% of taus are retained, while 98% of the multijet (MJ) background is rejected. In CDF boosted decision tree (BDT) based algorithms are used for the same purpose.

## 2. Jets, $b$ jets, and missing transverse energy

In CDF, jets are reconstructed using a calorimeter based clustering algorithm, with a cone of size  $\Delta R < 0.4$ . In D0, jets are reconstructed in the calorimeters for  $|\eta| < 2.5$  using the D0 run II iterative cone algorithm. Calorimeter energy deposits within a cone of size  $\Delta R < 0.5$  are used to form the jets. The energy of the jets is calibrated by applying a jet energy scale correction determined using  $\gamma$ +jet events.

Jet identification efficiency and jet resolutions are adjusted in the simulation to match those measured in data.

At high instantaneous luminosity, the jets are further required to contain at least two tracks with  $p_T > 0.5$  GeV associated with the primary vertex at D0.

At both CDF and D0, the identification of quarks initiated by a  $b$  quark (“ $b$  tagging”) is done in two steps [87]. The jets are first required to pass a taggability requirement based on charged particle tracking and vertexing information, to ensure that they originate from the interaction vertex and that they contain charged tracks. At D0 a  $b$  tagging NN is applied to the taggable jets. This NN uses a combination of seven input variables, five of which contain secondary vertex information; the number and mass of vertices, the number of and  $\chi^2$  of the vertex contributing tracks, and the decay length significance in the  $x - y$  plane. Two impact parameter based variables are also used. At CDF the next step in  $b$  tagging is done using a NN with similar variables but including additional track quality information [88]. The CDF experiment also employs a cut based secondary vertex tagger [89]. As an example at D0 the typical efficiency for identifying a  $p_T = 50$  GeV jet that contains a  $b$  hadron is  $(59 \pm 1)\%$  at a corresponding misidentification rate of 1.5% for light parton ( $u, d, s, g$ ) initiated jets. This operating point is typically used for events with two “loose” ( $L$ )  $b$ -tagged jets. When tightening ( $T$ ) the identification requirement, the efficiency for identifying a jet with  $p_T$  of 50 GeV that contains a  $b$  hadron is  $(48 \pm 1)\%$  with a misidentification rate of 0.5% for light parton jets. The event missing transverse energy ( $\cancel{E}_T$ ) is calculated from individual calorimeter cell energies in the calorimeter. It is corrected for the presence of any muons and all energy corrections to leptons or to the jets are propagated to  $\cancel{E}_T$ . Both experiments identify events with instrumental  $\cancel{E}_T$  by comparing missing transverse energy calculations based on either reconstructed tracks or calorimeter deposits. The CDF experiment employs an algorithm that combines tracking and calorimeter information to improve  $\cancel{E}_T$  resolution.

## IV. THE LHC, ATLAS, AND CMS EXPERIMENTS

The LHC accelerator is a proton-proton collider operating at the highest energies currently attained by a hadron collider, which started operation in 2010. During the 2011 data taking period it was configured to collide beams with 7 TeV center of mass energy and provided an integrated dataset of approximately  $5 \text{ fb}^{-1}$  to the LHC experiments, while during 2012 it was configured at 8 TeV and provided an integrated dataset of approximately  $5.8$  ( $5.3$ )  $\text{fb}^{-1}$  to ATLAS(CMS). The instantaneous luminosity of the LHC has reached  $7.7 \times 10^{33} \text{ cm}^2 \text{ s}^{-1}$  making 20-30 multiple interactions per crossing a typical occurrence and creating additional challenges for triggering on and reconstructing physics events. A proton-proton collider at high energy provides large cross sections for gluon-gluon or quark-quark initiated Higgs boson pro-

duction processes such as gluon fusion and vector boson fusion. For instance, the cross section for gluon fusion to a Higgs boson is increased by a factor of approximately 15 compared to the Tevatron. In addition, the increase in center of mass energy from 7 to 8 TeV correspondingly raises the Higgs boson cross section by an additional factor of approximately 30%.

The LHC experiments are forward-backward and cylindrically symmetric detectors with tracking, calorimetric and muon detector elements.

The ATLAS detector includes an inner tracking and vertexing system, electromagnetic and hadronic calorimetry and an outer muon detection system [90]. The inner tracking detector consists of a silicon pixel detector, a silicon micro-strip detector, and a transition radiation tracker immersed in the field of a 2 T solenoidal magnet which provides charged particle tracking and vertex finding over a large pseudorapidity range of  $|\eta| < 2.5$ . The inner tracker and solenoid is surrounded by a high-granularity liquid-argon sampling electromagnetic calorimeter which provides electron (photon) finding in the range  $|\eta| < 2.47$  ( $|\eta| < 2.37$ ). An iron-scintillator tile calorimeter provides hadronic coverage in the central rapidity range. The end-cap and forward regions are instrumented with liquid-argon calorimetry for both electromagnetic and hadronic measurements which extends jet finding to  $|\eta| < 4.9$ . The muon spectrometer surrounds the calorimeters and consists of three large superconducting toroids, each with eight coils, a system of precision tracking chambers, and detectors for triggering in the range  $|\eta| < 2.4$ .

The CMS detector consists of a barrel assembly and two endcaps, comprising, in successive layers outwards from the collision region, a silicon pixel and strip tracker, a lead tungstate crystal electromagnetic calorimeter, a brass-scintillator hadron calorimeter, a superconducting solenoid, and gas-ionization chambers embedded in the steel return yoke for the detection of muons [91]. The silicon detector provides charged particle tracking and vertexing for  $b$  tagging over a large pseudorapidity range of  $|\eta| < 2.5$ , which is well matched to the coverage of the barrel and electromagnetic calorimeter as well as that of the muon chambers providing coverage to  $|\eta| < 3$  and  $|\eta| < 2.4$  for electron and muon identification respectively. The return field of the magnet allows independent momentum measurement and triggering in the muon chambers. The identification of photons and  $\tau$  leptons in hadronic decay modes is performed within the overlapping pseudorapidity range of the tracker and electromagnetic calorimeter. Jet finding can be performed in an expanded pseudorapidity range up to  $|\eta| < 5.0$  using forward calorimeters.

Further detail about the primary systems of the experiments are given next.

## A. Tracking detectors

The ATLAS tracker consists of a silicon pixel and strip tracker and a transition radiation straw tube tracker immersed in a 2.0 T magnetic field provided by a solenoidal magnet. The strip tracker consists of four barrel layers and nine end-cap disks at each end. The pixel detector consists of three barrel layers and two end-cap disks at each end. The silicon inner detector tracks charged particles over the range  $|\eta| < 2.5$  typically adding three pixel hits per track and allowing for high efficiency primary vertex finding and  $b$ -jet identification. The transition radiation tracker consists of 4 mm drift tubes configured in a barrel region and two sets of multiple wheel endcaps. This configuration provides high efficiency  $r - \phi$  tracking with typically 36 hits per track in the range  $|\eta| < 2.0$ . Between the straws a gas mixture primarily consisting of xenon and carbon dioxide causes ultrarelativistic charged particles to produce transition radiation photons which are converted to electron-positron pairs in thin foils and leave much larger signals in some straws.

The central feature of the CMS detector is a 6 m internal diameter 3.8 T solenoidal magnet. The solenoid provides a uniform bending field for a large volume silicon strip and pixel tracker. The strip tracker consists of ten barrel layers and six end-cap disks at each end. The pixel detector consists of three barrel layers and three end-cap disks at each end. The tracker typically allows 12 or more hits to be found for all tracks, including three layers of pixel hits, and allows for high efficiency tracking for  $|\eta| < 2.5$  as well as high efficiency primary vertex finding and  $b$ -jet identification.

## B. Calorimeters

The ATLAS calorimeter uses sampling technologies over the entire angular area of coverage. The electromagnetic calorimeter is a lead-liquid argon (LAr) sampling calorimeter and is divided into overlapping barrel and end-cap portions with coverage up to  $|\eta| < 3.2$ . The calorimeter is divided into three barrels and two end-cap parts, with very fine granularity in their inner layers providing excellent angular resolution for electrons and photons. The barrel calorimeter has an extra inner LAr layer that functions as a preshower detector with high longitudinal segmentation. The mass resolution for diphotons with an invariant mass of 125 GeV is approximately 1.5 GeV. The system has sufficient angular pointing ability to loosely associate photons with a primary interaction vertex to reduce combinatoric backgrounds. The hadronic sampling calorimeter is divided into a barrel region and endcaps that cover the range up to  $|\eta| < 3.2$  with seven to ten interaction lengths of instrumented material. The barrel region is composed of steel absorber plates with scintillating tile readout. The end-cap calorimeters are based on LAr technology with copper absorber. A forward calorimeter based on copper



(inner) and tungsten (outer) sampling extends the pseudorapidity range to  $|\eta| < 5.0$ . The inner copper portion gives the forward calorimeter the ability to perform electromagnetic calorimetry.

CMS incorporates a lead tungstate crystal electromagnetic calorimeter and a brass and scintillator sampling hadronic calorimeter enclosed within the solenoid. The electromagnetic calorimeter is divided into a barrel region and two endcaps which extend coverage up to  $|\eta| < 3.0$ . The crystals have cross-sectional areas of  $22 \times 22 \text{ mm}^2$  in the barrel and  $29 \times 29 \text{ mm}^2$  in the endcap, and the calorimeter material has a Moliere radius of 21 mm leading to narrow showers and good angular resolution. The end-cap calorimeter has two layers of silicon detectors interleaved with lead layers configured as a preshower detector. The excellent energy and good angular resolution of the calorimeter gives a diphoton mass resolution of 1.1 GeV at a mass of 120 GeV. The hadronic sampling calorimeter is divided into a barrel region and endcaps that cover the range up to  $|\eta| < 3.0$  with 7 to 11 interaction lengths of instrumented material. In addition there is a tail catcher calorimeter located outside the solenoid which increases the material of the calorimeter to at least ten interaction lengths everywhere. An iron forward calorimeter readout by quartz fibers extends the pseudorapidity range to  $|\eta| < 5.0$  to improve measurement of transverse energy and detection of missing transverse energy.

### C. Muon systems

The ATLAS muon system is based on the magnetic deflection of muon tracks within large superconducting air-core toroid magnets, instrumented with separate trigger and high-precision tracking chambers. The magnetic field is generated by three toroids, one in the barrel region,  $|\eta| < 1.4$ , and two in the end-cap regions,  $1.6 < \eta < 2.7$ , with an overlapping region in between. This magnet configuration provides a field which is mostly orthogonal to the muon trajectories over the entire  $\eta$  range. Precision tracking is provided by monitored drift tubes and cathode strip chambers, while resistive plate chambers and thin gap chambers provide fast triggering capability based on independent measurements of the particle momentum for the central and forward regions respectively.

The CMS muon system makes use of three technologies interleaved in the steel return yoke of the magnet; drift tubes (central) and cathode strip chambers (forward) for precision tracking and triggering based on tracking information and resistive plate chambers for tracking and triggering based on time measurements. The return field of the solenoid saturates the return yoke providing a bending field for independently measuring muon momenta. The chambers are divided into four stations with 14 layers of drift tubes or six layers of cathode strip chambers for robust tracking.

### D. Triggering

Both detectors use a multilevel triggering system. The first level of the trigger allows for the measurement of the momentum or energy of physics objects including electrons and photons as electromagnetic energy deposits, muons with independent measurement of the momentum in the muon systems, jets and missing transverse energy using full calorimeter information, and taus as narrow jets. The event rate is reduced to approximately 100 kHz at the level one. The ATLAS experiment employs a second level trigger which repeats physics object identification using the full granularity of the detector and further reduces the event rate to 3.5kHz. Both detectors employ a full event reconstruction using optimized versions of offline reconstruction code running on commercial processors as a level three or high level event filter with an output rate of about 200 Hz for ATLAS and 500 Hz for CMS.

### E. Physics object identification at the LHC

Both experiments classify observed signatures in their detectors as physics objects that can be associated with the particles and decay products of particles produced in high-energy collisions. Physics analysis can be performed directly on these physics objects. The various physics signatures identified by the experiments are discussed next.

#### 1. Charged lepton identification

For electron identification both experiments use clusters formed in the electromagnetic calorimeters and associate them to tracks found in the tracker by matching to their extrapolated position and energy [92–94]. The clustering algorithm takes into account the typical spread of the cluster in  $\varphi$  due to bremsstrahlung photons. Tracks are generally identified using inside-out algorithms since the inner pixel detectors are the least occupied tracking system due to their high granularity. Electron candidates are required to pass requirements on cluster shape information, energy leakage information in the hadronic calorimeter, and track quality information. Different operating points are defined for different levels of selection efficiency and background rejection. Tighter operating points with lower efficiency and better background rejection include tighter criteria on identification requirements, requirements to reject electrons from photon conversions, and requirements on track impact parameter to reject electrons from interactions with matter or long-lived decays. The CMS experiment employs a BDT based multivariate electron identification algorithm for several analyses to improve efficiency and background rejection.

Because of the large bending fields in the muon spectrometers of the LHC experiments, muons can be

identified in the muon systems independently of the tracker [94–96]. In addition muons can be identified in the combined muon and tracking systems. Both experiments form combined tracker and muon system muons by associating independently reconstructed muons in the muon systems to charged tracks in the tracker using position and momentum information. CMS additionally identifies muons by extrapolating tracks into the muon system to perform an inside-out search for compatible muon system hits, which improves muon finding efficiency at low transverse momenta. Muons used in analysis are generally required to be identified in both systems, pass minimum tracker hit and muon system segment requirements, and satisfy requirements on track impact parameter to help reject decays to muons from long lived particles and cosmic rays.

Both experiments increase the purity of identified electrons and muons by requiring that the charged lepton candidates be isolated, which rejects real and misreconstructed charge leptons contained within jets. The ATLAS experiment applies relative calorimeter based isolation for electrons and relative tracker based isolation for muons based on the total calorimeter energy or track momenta found in a cone around the candidate divided by the transverse energy or momentum of the candidate. The CMS experiment applies relative particle flow based isolation based on charge tracks; electromagnetic energy from electrons, photons or neutral pions; and neutral hadronic energy not associated with tracks found in a cone around the candidate and divided by the transverse energy or momentum of the candidate. These ratios are required to be less than a given value which can be adjusted to achieve different levels of performance. The particle flow technique as used at CMS is described in more detail at the end of this section.

The identification of hadronically decaying  $\tau$  leptons is characterized by the presence of one or three charged hadrons, identified as tracks with associated calorimeter energy, and possible narrow strips of electromagnetic energy deposits characteristic of neutral pion decay to photons, all contained in a narrow collimated jet [97]. The ATLAS experiment combines this information together in a boosted decision tree based multivariate discriminant [98]. The CMS experiment uses a particle flow technique to measure the charged hadrons in the tracking detector and neutral pions as strip shaped electromagnetic energy deposits. It also improves the mass resolution of objects reconstructed as a hadronically decaying  $\tau$  by performing a fit constraining the objects from the  $\tau$  decay to the  $\tau$  lepton mass.

## 2. Photon identification

The identification of photons uses similar criteria to those used for electrons except that events with a track or track segment compatible with the electromagnetic cluster are rejected. Photon candidates are formed from

electromagnetic clusters in the EM calorimeter [99]. The clustering algorithm and subsequent identification criteria allows for the possibility that the photon converts to an electron pair. Photon candidates are required to pass requirements on cluster shape information and energy leakage information in the hadronic calorimeter. The ATLAS experiment additionally applies isolation requirements, while the CMS experiment includes the above criteria and isolation information in a BDT algorithm designed to reject non prompt sources of photons. The ATLAS experiment also uses the longitudinal segmentation of its EM calorimeter to require that the photons are compatible with pointing to the primary high transverse momentum interaction vertex. In cases of conversion early in the material of the tracker, both experiments reconstruct the electron-position conversion pairs when possible. In this case the vector sum of the track momenta are required to point toward the primary interaction vertex.

## 3. Light and heavy flavor jets

Jets are generally reconstructed using the anti- $k_t$  algorithm based on calorimeter clusters [100]. The excellent granularity of the LHC detectors allows for the effective use of such an iterative clustering-based jet-finding algorithm. Raw jet energy measurements are corrected for imperfect calorimeter response using correction factors from studies of detector response in test beam data, MC simulations, and collision data. In high pileup conditions jets can be required to point to the hard interaction vertex. Heavy flavor jets, or jets originating from  $b$  quarks, are found based on the positive track impact parameter significance of tracks and reconstructed secondary vertices [101, 102]. The ATLAS experiment combines the track impact parameter significance information to form a likelihood ratio quantifying whether a jet originates from a  $b$ -flavored parton or light parton. A second likelihood is formed using secondary vertex information including decay length significance and vertex mass information. The further use of a likelihood or similar technique allows the results of the two types of algorithms to be combined into a single continuous  $b$ -flavored jet identification variable. The experiments define multiple operating points with different selection efficiencies and background rejection. As an example using this type of information both experiments can achieve 50% efficiency with a factor of 1000 in background rejection.

## 4. Missing transverse energy

Both experiments use measurements of missing transverse energy to identify events with neutrinos [103, 104]. The ATLAS experiment measures the visible energy using electromagnetic clusters corrected for the average hadronic component and corrected for the transverse mo-

momentum of identified muons. The magnitude and direction of the missing transverse energy are obtained from the energy imbalance in the transverse plane. The CMS experiment uses a particle flow method to measure the visible energy and infers the  $\cancel{E}_T$  measurement in the same way. The  $\cancel{E}_T$  measurement can be improved in the presence of high pile-up by using associated objects to calculate the  $\cancel{E}_T$  for a given vertex. The excellent tracking efficiency and z coordinate resolution of the experiments are essential for this technique. In addition events with false  $\cancel{E}_T$  from jet mismeasurement are identified by methods such as checking whether the  $\cancel{E}_T$  is collinear with jets or charged leptons or comparing different methods of the  $\cancel{E}_T$  measurement such as those based solely on reconstructed charged tracks or calorimeter energy cluster information.

### 5. Particle flow

In CMS, jet and missing transverse energy reconstruction, and  $\tau$  lepton identification are substantially improved by using particle flow identification techniques [105, 106] that classify detector signatures as charged or neutral hadrons, photons, or charged leptons using combined information from the tracker, calorimeters, and muon detectors. Electrons, photons, and neutral pions are measured in the EM calorimeter. Muons are measured in the tracker and muon detectors. Tau leptons in decay modes involving hadrons are found combining tracker information for charged hadrons and EM information for neutral pions. Charged hadrons in jets are measured using the tracker. Neutral energy not associated with any of the above objects is measured as energy clusters in the EM and hadronic calorimeters. The vector sum of particle flow objects can also be used to identify missing transverse energy.

## V. TEVATRON LOW-MASS HIGGS BOSON SEARCHES

At lower masses ( $m_H < 135$  GeV), the dominant decay of the Higgs boson is  $H \rightarrow b\bar{b}$ , but it is hopeless to search for direct ( $gg \rightarrow H$ ) Higgs boson production in this decay mode, due to the overwhelming multijet background. However,  $q\bar{q}$  annihilation results in associated vector boson-Higgs boson production ( $VH$ ) in  $p\bar{p}$  collisions with a better signal-to-background ratio than available at a  $pp$  collider. The “primary” channels for searching for a low-mass Higgs boson at the Tevatron,  $WH$  and  $ZH$  production, are best studied in the  $\ell\nu b\bar{b}$ ,  $\ell\ell b\bar{b}$  or  $\nu\nu b\bar{b}$  final states. The lower branching ratios or poor signal to background of the other decay modes render their sensitivity smaller than these primary channels but are also searched for to provide additional sensitivity in the combination of all channels.

The associated production analyses generally proceed

in three steps. The first is preselection where a high statistics sample of events containing bosons and jets is constructed, allowing for detailed validation of background modeling. The  $W$  and  $Z$  are required to decay leptonically [topologies where  $W$  or  $Z$  decay hadronically are also searched for, but are less sensitive ([107])] to facilitate event triggering and selection. Electrons and muons (including those coming from taus decaying leptonically) allow for a relatively pure selection, but  $Z \rightarrow \nu\nu$  decays are also exploited. In the next selection step, at least one jet is required to be identified as a  $b$ -quark jet, enhancing the signal to background in separate final sub-samples defined by the number and type of  $b$ -quark jets found. In the final step, multivariate analysis techniques are applied to each of the samples to further separate the potential signal from the backgrounds.

Vector boson fusion production, associated production with vector bosons, and direct Higgs boson production can also be exploited when the Higgs boson decays to a  $\tau\tau$  pair, by making use of the kinematics of the potential additional jets in the final state. These processes suffer from significant background and so are considered as secondary channels at the Tevatron. Another secondary channel which is exploited at the Tevatron is inclusive production of a Higgs boson with Higgs boson decay to two photons. The sensitivity of this channel is low due to the small branching ratio of this decay, typically smaller than 0.2 %. The  $t\bar{t}H$  production is also searched for, but has low sensitivity.

In all the analyses, the data are separated into multiple orthogonal search samples of varying sensitivities. The analyses are described next and all results are summarized in section IX.

### A. $VZ$ with $Z \rightarrow b\bar{b}$ as a test of the $VH$ search

Since the low-mass analyses use advanced multivariate techniques for separating signal and backgrounds and are obtained from low signal-to-background search samples, a crucial test has been performed considering  $WZ$  and  $ZZ$  diboson production with  $Z$  decays to heavy flavor as signal, mimicking the final states of  $WH$  and  $ZH$  including the essential feature of resonant dijet production. In such analyses the  $WW$  process is taken as a background, with a normalization constrained to its NLO cross section. These analyses, and their combination, are performed in the same way as their Higgs counterparts. The CDF+D0 combination displays strong evidence ( $4.6\sigma$ ) for such production, with a measured cross section  $\sigma(VZ) = 4.47 \pm 0.97$  pb consistent with the SM prediction [108]. Evidence was first seen by both collaborations separately [109, 110] using 9.5 and 7.5  $\text{fb}^{-1}$  respectively.

### B. $WH \rightarrow \ell\nu b\bar{b}$

The search for the process  $q\bar{q} \rightarrow WH + X$  in which a quark-antiquark pair leads to the production of the Higgs boson in association with a  $W$  boson is based on a total integrated luminosity  $\mathcal{L} \simeq 10 \text{ fb}^{-1}$  of collision data collected by both the CDF and D0 detectors at the Fermilab Tevatron  $p\bar{p}$  collider between 2002 and 2011 [111–114]. Candidate  $W$  boson events are preselected via their decays to an electron or a muon plus a neutrino ( $W \rightarrow e$  or  $\mu\nu$ ) while the Higgs boson is identified through its decay mode into a pair of  $b$  quarks ( $H \rightarrow b\bar{b}$ ). The experimental signature is a single isolated lepton, missing transverse energy, and either two or three (to accommodate additional gluon radiation in the hard collision) jets, at least one of which is required to be consistent with having been initiated by a  $b$  quark.

To increase signal acceptance, the lepton identification criteria are as loose as possible. This results in backgrounds originating from MJ events, in which one of the jets is misidentified as an isolated lepton. In the CDF analysis, the MJ background is strongly reduced by kinematic cuts and by using a dedicated multivariate technique to reject this background [111]. The remaining MJ background contribution is modeled from the data using side-band techniques. In the D0 analysis, the MJ background contributions passing the preselection criteria in each sample are determined from the data using an unbinned matrix method approach [112]. The “physics” backgrounds with similar event topologies are modeled using Monte Carlo event generators. The SM predictions are used to set the relative normalizations of all of the generated samples, with additional normalization factors applied to samples of  $W$  bosons +  $n$  partons generated using the ALPGEN Monte Carlo event generator. These factors are determined at the preselection stage where the SM Higgs boson contribution is negligible. The predicted backgrounds model the data well in the high statistics sample before a  $b$ -tagging algorithm is applied, as shown in Fig. 5.

The CDF and D0 analyses proceed by subdividing the selected sample into orthogonal subsamples based on how many of the jets in the event, one or two, are consistent with having been initiated by a heavy  $b$ -quark, and at what level (“loose ( $L$ )” or “tight ( $T$ )”) of confidence. CDF has five tagging categories ( $TT, TL, LL, T, L$ ) for the two jet sample, and two categories ( $TT, TL$ ) for the three jet sample, while D0 uses four categories ( $TT, TL, LL, T$ ) and two categories ( $LL, T$ ) respectively. In two  $b$ -tagged jet events, the dominant remaining backgrounds are from  $Wb\bar{b}$ ,  $t\bar{t}$ , and single top-quark production. In single  $b$ -tagged jet events the dominant backgrounds are  $W$  + light or  $c$ -quark jet production as well as MJ background events. To further discriminate the remaining backgrounds from the signal, MVA techniques are applied to each subsample. Some of the discriminant variables used in these analyses are given in Table I.

Systematic uncertainties affect not only the normal-

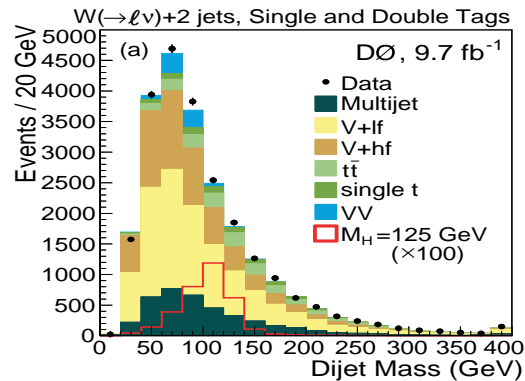


FIG. 5: Dijet mass distribution in the D0  $WH$  analysis for the  $W + 2$  jet sample with 1 or 2 identified  $b$ -jets. The data are well described by the sum of all the SM backgrounds. The simulated signal is also represented.

rf input variable	Description
$\cancel{E}_T$	Missing transverse energy
$M_W^*$	Lepton- $\cancel{E}_T$ transverse mass
$p_T(\ell - \cancel{E}_T \text{ system})$	$p_T$ of $W$ candidate
$p_T(j_1) p_T(j_2)$	Leading (subleading) jet $p_T$
$m_{jj}$	Dijet invariant mass
$p_T(\text{dijet system})$	$p_T$ of dijet system
$\Delta\mathcal{R}(j_1, j_2)$	$\Delta\mathcal{R}$ between jets
$\Delta\phi(j_1, j_2)$	$\Delta\phi$ between jets
$H_T$	Scalar sum of $p_T$ of all jets

TABLE I: Description of some characteristic kinematic input quantities of the MVA technique used in the  $WH$  analyses.

ization of the signal and backgrounds, but also the shape of the MVA output distributions. The influence of each source of systematic uncertainty is studied separately for each of the independent subsamples. Uncertainties in the efficiencies of selection, on jet calibration, and on the  $b$ -tagging criteria affect the precision at which the background modeling is known. The uncertainties on the parton density functions and the effect of renormalization and factorization scales on signal and background simulation are also taken into account. All these uncertainties are allowed to affect the shape of the MVA output distributions.

### C. $ZH \rightarrow \ell b\bar{b}$

The search by the CDF and D0 collaborations at the Tevatron for the process  $q\bar{q} \rightarrow ZH + X$  in which a quark-antiquark pair leads to the production of the Higgs boson in association with a  $Z$  boson decaying to a pair of charged leptons is also based on a total integrated luminosity  $\mathcal{L} \simeq 10 \text{ fb}^{-1}$  [115–118]. Candidate  $Z$  boson events are preselected via their decays into  $e^+e^-$  or  $\mu^+\mu^-$  pairs, and the associated Higgs boson is identified through its decay into a pair of heavy  $b$ -quarks ( $H \rightarrow b\bar{b}$ ). Candidate events are required to have two or three jets, at least one of which is identified as a  $b$  jet.

In this final state, which requires two leptons, the MJ background is negligible. The physics backgrounds are modeled using the same Monte Carlo event generators used in the  $WH$  analysis.

To maximize the lepton acceptance and benefit from higher quality lepton categories, the events are classified according to the lepton types. Those having both leptons identified with high confidence are treated separately from the others which contain loosely identified, forward, or track-based leptons. These samples are analyzed independently, allowing for an optimal sensitivity of the search. In addition, multivariate lepton selections are used. In CDF, to enhance the discriminating power of the dijet invariant mass, a NN derived energy correction is applied to the jets. This correction depends on the missing transverse energy and its orientation with respect to the jets. In D0, jet energy resolution improvements are obtained through a kinematic fit of the complete event, since all particles can be detected in this process.

These analyses also proceed by subdividing the selected sample into orthogonal subsamples based on the number and the quality of the  $b$ -tagged jets in the event. CDF has four tagging categories ( $TT, TL, LL, T$ ) for both the  $Z + 2$  and  $Z + 3$  jet samples, while D0 has a different treatment using two tagging categories ( $TL, T$ ) for the  $Z + 3$  jet sample. CDF employs two NNs to simultaneously separate signal events from the dominant  $Z$ +jets and kinematically different  $t\bar{t}$  backgrounds. These NNs use various kinematic distributions, matrix element probabilities, and the output of a separate jet flavor separating NN as inputs. In single and double  $b$ -tagged jet events, the dominant remaining background is  $Zb\bar{b}$ . To suppress the remaining background MVA techniques are applied to each subsample. Systematic uncertainties are overall less important than for  $WH$  since no missing transverse energy is involved, but most of the other systematic uncertainties are of similar magnitude to those of the  $WH$  analyses.

#### D. $ZH \rightarrow \nu\nu b\bar{b}$ and $VH \rightarrow \cancel{E}_T b\bar{b}$

The remaining  $b\bar{b}$  analysis is built to detect the  $ZH \rightarrow \nu\nu b\bar{b}$  process but is also sensitive to  $WH$  events in which the charged lepton is not identified, hence its alternate label as  $VH \rightarrow \cancel{E}_T b\bar{b}$ . These searches are based on a total integrated luminosity  $\mathcal{L} \simeq 10 \text{ fb}^{-1}$  [119–122]. Since this final state contains no leptons, triggering on these events and modeling the effects of the trigger requirements on the event selection are significant challenges. Both CDF and D0 use triggers based on  $\cancel{E}_T$ , with or without accompanying jets. The analyses are performed while studying in parallel several control samples to monitor the understanding of the background. Events are required to have significant  $\cancel{E}_T$  and two or three jets, well separated from the  $\cancel{E}_T$  direction. For the preselection, multivariate approaches are also applied to the events to remove a large part of the MJ background. For the final selection  $b$  tag-

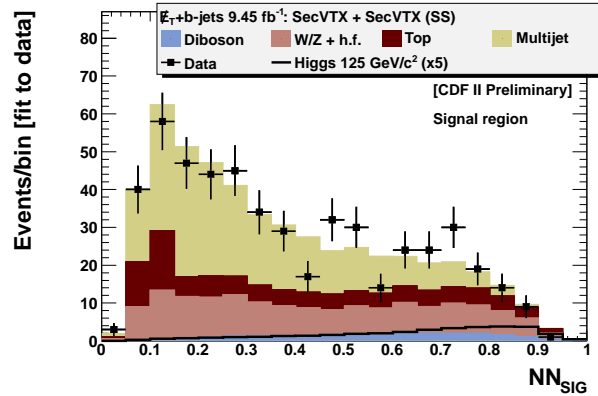


FIG. 6: Distribution of the NN discriminant in the CDF  $\cancel{E}_T b\bar{b}$  analysis for the sample with two or three jets where 2 of the jets are tagged as  $b$  jets by the secondary vertex algorithm. The data are well described by the sum of all the SM backgrounds. The simulated signal is also represented.

ging is employed.

For this analysis, the preselection plays a crucial role, given the size of the MJ background. As an example, at D0, the preselection uses the following main requirements. The events must have a well-reconstructed interaction vertex and two or three jets with associated tracks to ensure efficient operation of the  $b$ -tagging algorithm. These jets must have  $p_T > 20 \text{ GeV}$  and  $|\eta| < 2.5$  and not be back-to-back in the transverse plane.  $\cancel{E}_T$  must be greater than 40 GeV, with large significance, i.e. with  $\cancel{E}_T$  values that are less likely to have originated from fluctuations in jet energies, and the scalar sum of the two leading jet  $p_T$  must be greater than 80 GeV.

The dominant signal topology is a pair of  $b$  jets recoiling against the  $\cancel{E}_T$  due to the neutrinos from  $Z$  decay with the direction of the  $\cancel{E}_T$  at large angles relative to both jet directions. Conversely, in the case of events from MJ background with fluctuations in jet energy measurements, the  $\cancel{E}_T$  tends to be aligned with a mismeasured jet. An alternate estimate of  $\cancel{E}_T$  can be obtained from the missing  $p_T$  calculated from the reconstructed charged particle tracks. This variable is less sensitive to jet energy measurement fluctuations and, in signal events, is also expected to point away from both jets, while in the MJ background its angular distribution is expected to be more isotropic. A variable characterizing these features is used to further reject the MJ background. As for the other  $b\bar{b}$  analyses, the physics backgrounds are taken into account using Monte Carlo event generators.

The preselected samples are subdivided into orthogonal subsamples based on the number and the quality of the  $b$ -tagged jets in the event. CDF has three tagging categories ( $SS, SJ, S$ ) for the analyzed two and three jet samples, where  $S$  represents a jet identified by a reconstructed secondary vertex, and  $J$  represents a jet identified by the presence of tracks not pointing to the main interaction vertex. D0 has two tagging categories for its two jet sample ( $TT$  and  $LL$  or  $T$ ). To suppress the

remaining backgrounds multivariate discriminant techniques are applied to each subsample as in Fig. 6.

### E. CDF and D0 results on $H \rightarrow b\bar{b}$ searches

Here we present the individual results from each collaboration. The results are extracted using the MVA discriminant distributions from each subchannel of these three  $H \rightarrow b\bar{b}$  analyses, and then combined. The CDF+D0 combination is discussed in Sec. IX. Here we present the results of each collaboration, while the limits for the three different search topologies are given in Table IV. The statistical techniques used are described in Sec. IX and allow for the extraction of the limit on the signal cross section normalized to the SM expectation, or, in case of excess, determine the  $p$ -value of the background fluctuation. At very low mass, when combining the three  $H \rightarrow b\bar{b}$  topologies, CDF and D0 exclude at 95% C.L. Higgs bosons with masses smaller than 96 and 102 GeV, respectively. However, in the results from both collaborations an observed limit above the background-only expectation is obtained for the  $\simeq 120$ -140 GeV range. In particular, the expected or observed limits at  $m_H = 125$  GeV are 1.8 or 4.2 and 2.3 or 3.2 times the SM expectation, for the CDF [123] and D0 [124] searches, respectively. To quantify the excess, the local  $p$  values are calculated and found to be minimal for a Higgs boson mass of 135 GeV at CDF and D0, where the local significance of these deviations with respect to the background-only hypothesis is  $2.7\sigma$  ( $1.7\sigma$ ), which themselves correspond to  $2.5\sigma$  ( $1.5\sigma$ ) global significances after applying look-elsewhere factors (cf. Sec. IX). These two mass values are compatible given the resolution of the dijet mass in these final states.

### F. Searches in $\tau_h$ final states

Higgs boson searches using tau leptons decaying hadronically ( $\tau_h$ ) complement those using electrons and muons. CDF performs a generic analysis searching for Higgs bosons decaying to  $\tau$  lepton pairs originating from direct  $gg \rightarrow H$  production, associated  $WH$  or  $ZH$  production, and vector boson fusion production [125]. A final state consisting of one leptonic  $\tau$  decay and one hadronic  $\tau$  decay or two leptonic  $\tau$  decays of different flavors  $e\mu$  is required. CDF hadronic  $\tau$  identification is performed using an MVA approach. The final discriminant for setting limits is obtained combining the output of four MVAs trained to separate a potential signal from each of the four primary backgrounds ( $Z \rightarrow \tau\tau$ ,  $t\bar{t}$ , multi-jet, and  $W$ +jet production). CDF also has an analysis of events that contain one or more reconstructed leptons ( $\ell = e$  or  $\mu$ ) in addition to a  $\tau$  lepton pair focusing on associated production where  $H \rightarrow \tau\tau$  and additional leptons are produced in the decay of the  $W$  or  $Z$  boson [126]. Events are separated into five separate analysis channels

( $\ell\ell\ell$ ,  $e\mu\tau_h$ ,  $\ell\ell\tau_h$ ,  $\ell\tau_h\tau_h$ , and  $\ell\ell\ell\ell$ ). The four lepton category includes  $\tau_h$  candidates. The final discriminants are likelihoods based on outputs obtained from independent MVA trained against each of the primary backgrounds ( $Z$ +jets,  $t\bar{t}$ , and dibosons).

The D0  $\ell\tau_h jj$  analyses also include direct  $gg \rightarrow H$  production, associated  $WH$  or  $ZH$  production, and vector boson fusion production [127, 128]. Decays of the Higgs boson to tau,  $W$ , and  $Z$  boson pairs are considered. A final state consisting of one leptonic  $\tau$  decay, one hadronic tau decay, and two jets is required. Both muonic and electronic subchannels are considered. The outputs of boosted decision trees are used as the final discriminant.

### G. Searches in $H \rightarrow \gamma\gamma$

Both CDF [129] and D0 [130] searched for Higgs bosons decaying into diphoton pairs with the full statistics ( $10 \text{ fb}^{-1}$ ). The CDF analysis searches for a signal peak in the diphoton invariant mass spectrum above the smooth background originating from QCD production in several detector based categories with different signal-to-background ratios. In the D0 analysis the contribution of jets misidentified as photons is reduced by combining information sensitive to differences in the energy deposition from real or false photons in the tracker and in the calorimeter in a neural network output ( $\text{NN}_o$ ). The output of an MVA, rather than the diphoton invariant mass, is used as the final discriminating variable. The final MVA takes as input variables the  $\text{NN}_o$ , the transverse energies of the leading two photons and the azimuthal opening angle between them, the diphoton invariant mass and transverse momentum, and additional variables, bringing an improvement in sensitivity of  $\approx 20\%$ .

### H. Searches for $t\bar{t}H$ production

The  $t\bar{t}H$  production is interesting for the direct  $tH$  coupling it involves, however its cross section is too small at the Tevatron to contribute strongly to the overall search sensitivity. CDF uses several nonoverlapping sets of events to search for the process  $t\bar{t}H \rightarrow t\bar{t}b\bar{b}$ . Events with a reconstructed lepton, large missing transverse energy, and four, five, and six or more jets are further subdivided into five  $b$ -tagging categories [131]. Neural network discriminants are used to set limits. Events with no reconstructed lepton [132] are separated into two categories, one containing events with large missing transverse energy and five to nine reconstructed jets and another containing events with low missing transverse energy and seven to ten reconstructed jets. A minimum of two  $b$ -tagged jets is also required and events with three or more  $b$  tags are analyzed separately from those with exactly two tags. Neural network discriminants are used to reject large MJ background contributions and separate potential  $t\bar{t}H$  signal events from  $t\bar{t}$  background events.

## VI. TEVATRON HIGH MASS HIGGS BOSON SEARCHES

As the hypothesized source of electroweak symmetry breaking, the Higgs boson has strong coupling to both massive electroweak bosons. At Higgs boson masses above 135 GeV the decay to a pair of  $W$  bosons is dominant, but even below the threshold to produce on-shell  $W$  bosons, the decay rate to one real and one virtual  $W$  boson is substantial. Both experiments pursue a strategy of searching for  $H \rightarrow W^+W^{-(*)}$  decay in final states with at least one charged lepton and from all production processes with substantial cross section. In addition, searches for the subdominant decay  $H \rightarrow ZZ$  are performed. The high-mass search has similar sensitivity to the individual searches for associated Higgs boson production with a  $W$  or  $Z$  boson performed using the  $H \rightarrow b\bar{b}$  decay mode at a Higgs boson mass of 125 GeV. As proof of principle the experiments have observed all of the direct diboson production processes with pairs of heavy gauge boson in final states that are topologically similar to those used in the Higgs boson search.

### A. Diboson analysis: $WW$ , $WZ$ and $ZZ$

At the Tevatron, the diboson analyses in final states with charged leptons are performed using the same techniques used in the high mass Higgs boson search. The diboson searches based on leptonic and semileptonic decay modes allow for testing analysis techniques and developing further understanding of the primary backgrounds to the Higgs boson search. The direct SM production of the  $WW$  [133, 134],  $WZ$  [135], and  $ZZ$  [136] have been observed in leptonic decay modes with two charged leptons, three charged leptons and four charged leptons respectively. The diboson searches have also been performed with larger datasets using the most modern lepton selections, providing measurements of the  $WW$  [137, 138]  $WZ$  [139, 140] and  $ZZ$  [140, 141] cross sections. The combined production of  $WW$  and  $WZ$  boson pairs has been observed in events with one charged lepton and jets [142] and such an approach has been applied to perform another high-mass Higgs boson search [143]. The combined production of all pairings of massive vector bosons has been observed in events with one vector boson decaying leptonically and the other hadronically [144].

### B. Analysis Topologies

The analysis requirements typically require a triggered lepton with  $p_T > 20$  GeV, possibly additional leptons with lower thresholds, and significant  $\cancel{E}_T$  that is not aligned along the direction of other physics objects in the events. The events are then categorized into a large number of topologies that are consistent with various Higgs boson production and decay modes. These topologies are

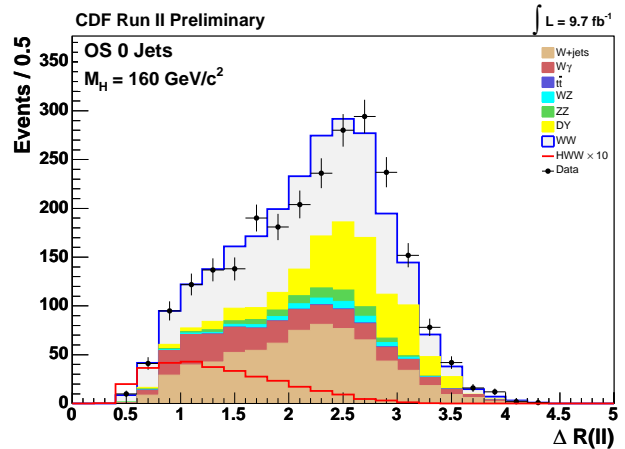


FIG. 7: The angle between the lepton candidates in three dimensions: The distribution of this angle for background and a  $H \rightarrow WW$  signal with  $m_h = 165$  GeV are compared

characterized by the number of charged leptons, whether the leptons are the same or opposite charge, and the number of jets. Each topology involves a limited set of dominant signals and backgrounds allowing for optimal discrimination, and is therefore analyzed separately. The most sensitive analysis topology involving zero jets and leptonic  $H \rightarrow W^+W^-$  is described in detail below, while the subdominant modes are briefly discussed afterward.

i)  $ggH \rightarrow W^+W^- \rightarrow \ell^+\nu\ell^-\bar{\nu} + n_{jet}$  [145, 146]. When  $n_j = 0$ , the signature is two opposite sign leptons,  $\cancel{E}_T$ , and no observed jets. The signal in this final state is almost 100% produced by the  $ggH$  process. The dominant background is from SM direct  $WW$  production with minor contributions from Drell-Yan production, the  $WZ$  and  $ZZ$  diboson processes where one or more charged leptons are not detected, and  $W$ +jets or  $W$ + $\gamma$  where a jet is misidentified as a lepton or the  $\gamma$  converts to an electron-positron pair, only one of which is detected. The strongest discriminant is the opening angle between the leptons in two dimensions (2D)  $\Delta\phi$  or three dimensions (3D)  $\Delta R$  (Fig. 7), due to the spin correlation between the two spin one  $W$  bosons when decaying from the scalar Higgs boson. The collinear topology of the charged leptons also results in a low dilepton invariant mass while Drell Yan background peaks at the  $Z$  mass and other backgrounds at large mass. The neutrinos are also collinear leading to larger  $\cancel{E}_T$ . Matrix element probabilities are effective discriminants because in the zero jet topology the final state of either Higgs boson or SM direct  $WW$  production is well described by a leading order matrix element. The transverse mass of the Higgs boson can be well reconstructed since the neutrinos are also collinear. The D0 experiment further subdivides this mode by lepton flavor. CDF subdivides this analysis into modes with two well-identified leptons, or one well-identified lepton plus and an isolated track, and analyzes events with low dilepton invariant masses as a separate

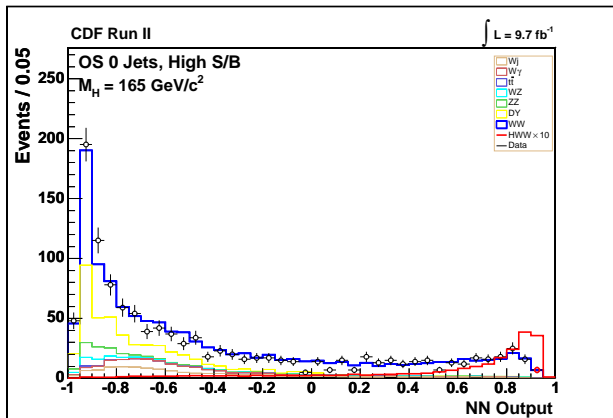


FIG. 8: NN discriminant for  $ggH \rightarrow WW \rightarrow \ell\nu\ell\nu + 0$  jet at CDF. The distribution for background and a  $H \rightarrow WW$  signal with  $m_H = 165$  GeV (multiplied by 10) are compared.

category.

When  $n_j = 1, 2$ , the signature is two opposite sign leptons,  $\cancel{E}_T$ , and observed jets. These topologies have substantial contributions from  $VH$  or  $VBF$  where the jets are observed from either one of the vector boson decays or final state quarks respectively and additional background from top pair production.

ii)  $VH \rightarrow VW^+W^- \rightarrow \ell^+X\ell^+\nu+X$  [147, 148]. Associated production events can result in events with either same sign leptons or trileptons when the associated vector boson decays to charged leptons. The background includes  $W$ +jets with a misidentified lepton in the same sign mode and SM direct  $WZ$  production in the trilepton case.

iii)  $(ggH, VH, VBF) \rightarrow H \rightarrow WW \rightarrow \ell\nu + \geq 2$  jet. Higgs boson production can be searched for inclusively in events where one of the  $W$  bosons decays leptonically and the other  $W$  boson decays to two quark jets [149]. The dominant backgrounds are from  $W$ +jets and multi-jet background where a jet is misidentified as a lepton.

iv) Other decay modes: The CDF and D0 experiments also consider modes where one  $W$  boson decays to a  $\tau$  lepton which decays hadronically [150].

Finally a search for the Higgs boson is performed in the  $H \rightarrow ZZ$  mode where both  $Z$  bosons decay to charged leptons [151]. The only significant background in this mode is SM direct  $ZZ$  production. The Higgs boson can be detected by looking for a narrow resonance in the four lepton invariant mass distribution. D0 includes acceptance for  $H \rightarrow ZZ$  in other cases where less than four charged leptons are found in the above searches.

### C. CDF and D0 results at high Higgs boson mass

All these search channels select a total of approximately 75 Higgs boson events per detector for a Higgs boson mass of 165 GeV. More than half of these events are

distinguished from the background with a good signal-to-background ratio using MVA discriminants as illustrated in Fig. 8. Examining the  $\Delta R$  distribution (Fig. 7) shows that the largest discriminating power comes from the spin correlation variable, due to the unique scalar nature of the Higgs boson.

No significant excess is seen in any of the high-mass Higgs boson search modes and limits are thus extracted, taking into account systematic uncertainties. The theory uncertainties become larger in events with more jets since, for instance, in the NNLO calculation, events with two additional jets are calculated only at NLO accuracy. These uncertainties are addressed following the treatment by [152, 153] and included in the limit extraction.

The expected limits with respect to the SM expectation for each experiment using the combination of all high-mass Higgs boson search topologies at  $m_H = 165$  GeV are 0.69 and 0.72 times the SM Higgs boson cross section for the CDF [154] and D0 [155] searches, respectively. The experiments each achieve expected sensitivity within a factor of approximately 1.5 of the SM cross section, in the mass range  $m_H = 140 - 185$  GeV. The CDF (D0) analysis excludes the SM Higgs boson in the mass range  $m_H = 148 - 175$  GeV (157 - 172 GeV). Additionally these searches provide strong sensitivity to the production of a Higgs boson at lower masses. The expected or observed limits at  $m_H = 125$  GeV are 3.1 or 3.0 and 3.6 or 4.6 times the SM Higgs boson cross section for the CDF and D0 searches, respectively. The limits for the different search topologies at  $m_H = 125$  GeV are given in Table IV.

## VII. LHC SEARCHES IN BOSONIC HIGGS BOSON DECAYS

The Higgs boson searches at the LHC are performed by decay mode. In this section we discuss each search separately, while the combination of all search results for each experiment is discussed in Sec. IX. Previous searches at LEP, Tevatron, and the LHC, in addition to indirect constraints indicated that the SM Higgs boson had a low mass between approximately 115 and 130 GeV with the region around 125 GeV being of highest interest. As of 4 July 2012 the LHC experiments had analyzed searches sensitive to this mass range and higher masses using datasets of approximately  $5 \text{ fb}^{-1}$  at 7 TeV and  $5.8 (5.3) \text{ fb}^{-1}$  for ATLAS (CMS) at 8 TeV.

### A. LHC diboson physics

The key modes for observing the Higgs boson at low mass are the fully reconstructed  $\gamma\gamma$  and  $ZZ$  decay modes. To explore the role of the Higgs boson in electroweak symmetry breaking the  $WW$  decay mode is also crucial. Understanding the non-resonant continuum production of these final states is important to control backgrounds



in the Higgs boson searches. The LHC experiments have observed  $\gamma\gamma$  production in 7 TeV  $pp$  collisions [156].  $WW$  [157–162] and  $ZZ$  [163–166] production has been observed in both 7 and 8 TeV collisions and their cross sections measured. These measurements typically use identical selections and techniques to those of the Higgs searches. Large samples have been collected in each decay mode. With future data samples the  $WW$  and  $ZZ$  modes can be used to study the electroweak symmetry breaking related phenomena of longitudinal vector boson scattering. The contribution of Higgs boson exchange to this process should limit the otherwise divergent behavior of this process at high energy.

## B. Searches in $H \rightarrow \gamma\gamma$

The LHC experiments have the ability to reconstruct a Higgs boson in the two photon decay mode [167–170]. The detectors are designed with the excellent energy and position resolution necessary to accurately reconstruct the invariant mass of two photon events. Excellent mass resolution is critical since backgrounds from multijet, multijet+photon, and photon+photon events are large. This decay has a small branching ratio, since the Higgs boson can decay only to photons through a loop diagram involving massive charged particles. The large inclusive production cross section at lower masses makes this a viable mode for a Higgs boson observation at low mass. In addition, observation of this mode would rule out spin 1 for the observed object.

Data are collected with diphoton triggers. Energy and isolation requirements are made on the photons to reduce backgrounds. Converted photons are also used and provide good energy and position resolution when electron pairs can be reconstructed by the trackers. The ATLAS experiment reduces background by using the longitudinal segmentation of the calorimeters to select photons that point to the hard interaction vertex.

Both experiments apply a separate selection for events with two forward jets to focus on a vector boson fusion like topology which has excellent sensitivity achieving a signal to background that is an order of magnitude greater than in topologies without forward jets typical of gluon fusion production. In the ATLAS experiment, to optimize sensitivity, events are further divided by whether photons are converted or not and by which pseudorapidity region of the detector they are reconstructed in, since these classes result in different diphoton mass resolution and as a result different signal to background. Finally, events are classified by the transverse momentum of the diphoton system since backgrounds are substantially reduced at high values. In the CMS experiment the output of a dedicated photon identification BDT, the transverse momentums of the photons, the opening angle between the photons, the pseudorapidity of the photons, and the estimated mass resolutions of the diphoton system are used to classify events by expected signal-

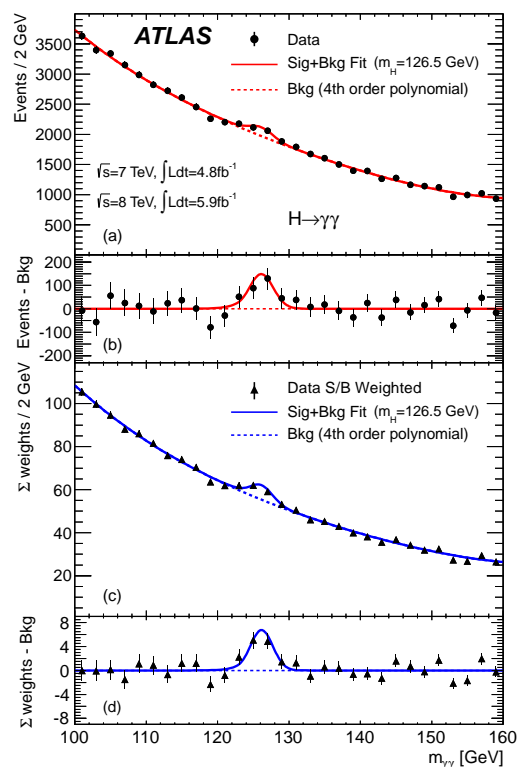


FIG. 9: Invariant mass of diphoton events in the ATLAS experiment. The results are presented with and without event weighting by an expected signal-to-background ratio.

to-background ratios using a BDT multivariate discriminate. An investigation of the categories formed by selecting on the BDT output indicates that divisions based on the transverse momentum of the diphoton system, the detector pseudorapidity region of the photons, and whether the photons are converted or unconverted largely determines the classification of events.

The sensitivities of the individual categories are taken into account when calculating the overall sensitivity of the analysis and when determining exclusions or signal significances. The collaborations weight events by expected signal-to-background ratio when displaying the diphoton mass distribution to give a visual representation of the benefit of this classification.

Using the two photon invariant mass distribution to search for the Higgs boson, regions at both low mass and higher mass have been excluded by both experiments leaving only a narrow region of mass unexcluded. The ATLAS experiment excludes the regions 112–122.5 and 132–143 GeV. This exclusion extends the lower exclusion bound of the LHC searches below the upper exclusion bound from the LEP searches, and when combined with other searches excludes the entire mass range below 600 GeV except for the narrow allowed region around 125 GeV.

These analyses have a strong sensitivity to the production of a low-mass Higgs boson of around 125 GeV with

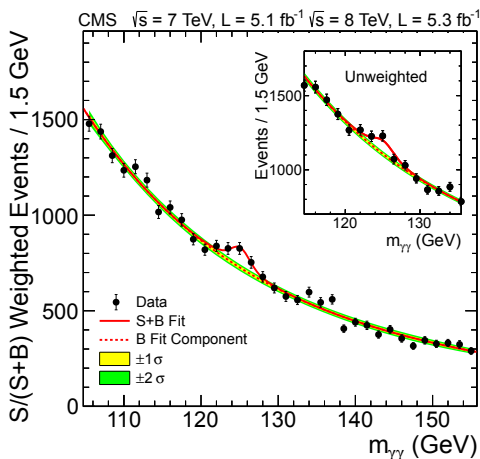


FIG. 10: Invariant mass of diphoton events in the CMS experiment with events weighted by an expected signal-to-background ratio and the unweighted distribution shown as an inset.

the expectation of observing approximately 200 events per experiment at that mass. In that region both experiments see a significant excess of events. The ATLAS diphoton invariant mass distributions both weighted by signal-to-background ratio and unweighted are shown in Fig. 9. The corresponding CMS diphoton invariant mass distributions are shown in Fig. 10.

The ATLAS experiment sees a  $4.5\sigma$  excess of events compatible with a narrow resonance of mass 126.5 GeV with a signal strength of  $1.9 \pm 0.5$  times the SM expectation. The CMS experiment sees a  $4.1\sigma$  excess of events compatible with a narrow resonance of mass 125 GeV with a signal strength of  $1.6 \pm 0.4$  times the SM expectation. The strong evidence seen by both experiments in this single decay mode indicates that a new boson has been observed and strongly disfavors spin one as a possible spin value. Further characterization of this excess is given next.

### C. Searches in $H \rightarrow ZZ \rightarrow \ell^+ \ell^- \ell^+ \ell^-$

Unique to the LHC experiments is the ability to observe the Higgs boson over a large range of masses through inclusive production and  $H \rightarrow ZZ \rightarrow \ell^+ \ell^- \ell^+ \ell^-$  decay [171–174]. In the CMS search the charged leptons from  $Z$  decay considered at 7 TeV include the  $\tau$  leptons [175]. The LHC experiments are designed to provide large angular coverage for lepton identification in order to detect events in this mode at an adequate rate. Because of the excellent lepton momentum resolution of the experiments, the Higgs boson mass can be reconstructed with sufficient precision that background rates are very low and event counts on order of 10 events are sufficient for discovery. With the assumption of SM production

rate the coupling to the  $Z$  boson can be measured, and, by comparison with the  $WW$  mode, the ratio of  $W$  and  $Z$  couplings can be measured. Finally, with larger data samples than reported here, the spin and parity of a possible Higgs boson can be determined solely from this mode using an angular analysis of the decay products.

Data are collected using single and dilepton (CMS) triggers. Transverse momentum requirements are made on the leptons to reduce backgrounds. Advanced techniques such as multivariate lepton identification are applied to maximize lepton finding efficiency. The CMS experiment improves mass resolution by using an algorithm designed to detect and recover the momentum of final state photons radiated by the leptons. ATLAS incorporates a similar technique as part of its electron momentum fit. In ATLAS one opposite charge same flavor pair of leptons is required to be consistent with the  $Z$  boson mass. After these requirements the most significant background is direct SM  $ZZ$  production. A Higgs boson signal can be distinguished from the background by looking for a narrow resonance in the four lepton invariant mass distribution. For a Higgs boson mass of 125 GeV the ATLAS and CMS experiments expect  $\simeq 10$  events each.

The performance of the four lepton search including selection efficiency estimates and the scale and resolution of the four lepton invariant mass is tested by both experiments by searching for the four lepton final state produced by a  $Z$  boson where one initial decay lepton radiates a photon which converts to a lepton and antilepton pair  $Z \rightarrow 4\ell$ . With looser selection on lepton transverse momentum and the dilepton masses of same flavor opposite sign pairs this mode can be detected with substantially higher statistical precision than a Higgs boson at lower mass. Both experiments perform this analysis within the framework of the Higgs boson search analysis and observe this decay with the expected performance [172, 174, 176].

In both experiments the dominant SM  $ZZ$  background is estimated from simulation normalized to NLO cross section predictions. In ATLAS the background from  $\ell^+ \ell^- + X$  events, which is dominated by  $Z + b\bar{b}$  and  $t\bar{t}$  events, is estimated by measuring the normalization of these backgrounds using selections designed to select non-prompt muons or nonisolated electrons, which are more likely to originate from  $b$  jets, and using a transfer factor from simulation to extrapolate the background prediction to the signal region. In CMS the backgrounds from  $Z + X$  events and  $t\bar{t}$  are estimated in a control region with one same flavor opposite charge dilepton pair with an invariant mass consistent with the  $Z$  boson and additional objects. Using a subset of events from this region with one additional identified lepton the probability for an object to be falsely identified as a charged lepton from  $Z$  decay is measured. That misidentification rate is applied to determine the number of events with a  $Z$  boson and two additional lepton candidates that are not from  $Z$  boson decay in the signal region.

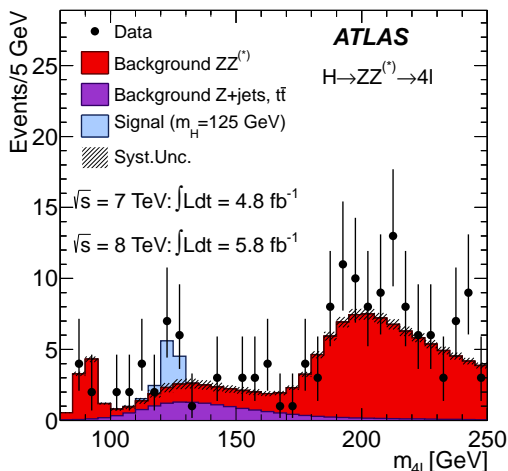


FIG. 11: The four lepton invariant mass distribution from the ATLAS experiment. The data are displayed as point and the background expectation as a histogram. Several SM Higgs boson signal contributions are included for different hypothetical Higgs boson masses. Background  $Z$ +jets and  $t\bar{t}$  bottom, background  $ZZ$  middle and Higgs boson signal top.

Both experiments use the four lepton invariant mass distribution to search for a Higgs boson. CMS further uses angular information based on the expected scalar spin zero and parity even nature of the Higgs boson in a matrix element likelihood analysis (MELA). Based on the searches large regions at high mass are excluded. The ATLAS experiment excludes the regions 131-162 and 170-460 GeV, while the CMS experiment excludes the regions 131-162 and 172-525 GeV. These are the largest exclusions from a single analysis channel, failing to exclude only the mass region where the  $WW$  branching ratio dominates just above the on-shell  $WW$  production threshold, and in the low-mass region.

These analyses have strong sensitivity to the production of a low-mass Higgs boson of roughly 125 GeV, as can be seen from the four lepton mass distribution from ATLAS, shown in Fig. 11, and from the invariant mass distributions of the four lepton candidates versus the MELA discriminant from CMS shown in Fig. 12.

Both experiments see a significant excess of events. The ATLAS experiment sees a  $3.4\sigma$  excess of events compatible with a narrow resonance of mass 125 GeV with a signal strength of 1.3 times the SM expectation. The CMS experiment sees a  $3.2\sigma$  excess of events compatible with a narrow resonance of mass 125.6 GeV with a signal strength of approximately 0.7 times the SM expectation. The evidence presented by both experiments of a narrow resonance with decays to  $ZZ$  indicates that a new boson has been observed, and the use of angular information to enhance the signal in the CMS case weakly favors spin zero and parity even as quantum numbers for the new boson though no definitive measurement of these properties is yet possible. Further characterization of this excess is

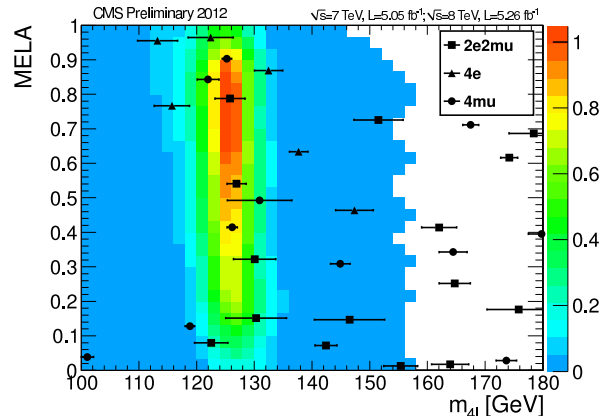


FIG. 12: A two-dimensional plot of four lepton invariant mass versus matrix element likelihood from the CMS experiment. Data are shown with event by event mass uncertainties while the expectation of a 125 GeV SM Higgs boson is superimposed as a temperature plot. The central region around 125 GeV is highest in probability.

given next.

#### D. Searches in $H \rightarrow W^+W^- \rightarrow \ell^+\nu\ell^-\bar{\nu}$

The LHC experiments search for inclusive Higgs boson production with the decay  $H \rightarrow W^+W^- \rightarrow \ell^+\nu\ell^-\bar{\nu}$  [177–180]. The decay is not fully reconstructed because of the neutrinos in the final state. However, the observation of collinear charged leptons in this decay mode is a distinct signature for the decay of a scalar particle. Observation of the Higgs boson in this decay mode also excludes spin one as a potential spin state. Also, using the production rate from theory, the mode can be used to determine the Higgs boson coupling to the  $W$  boson or the ratio of  $W$  and  $Z$  couplings through comparison with the  $H \rightarrow ZZ$  mode. In addition, by comparing events with zero or one jet to events with two forward jets, the gluon fusion and vector boson fusion production rates can be compared.

The data for the searches are collected using single lepton triggers (ATLAS) and dilepton triggers (CMS). Requirements are made on the transverse momentum of the charged lepton candidates, the magnitude of the missing transverse energy and on the  $\cancel{E}_T$  direction, which must not be collinear with other physics objects in the event. Also  $\cancel{E}_T$  measured using the calorimeter and tracker are compared to require compatibility and reject events with false  $\cancel{E}_T$ . Loose selection on the collinearity of the charged leptons is imposed to be consistent with the decay of a spin zero object to a  $W$  boson pair with subsequent leptonic decays.

ATLAS considers only electron and muon events, since such final state does not have significant Drell-Yan backgrounds and is substantially more sensitive. CMS divides events into same flavor, electron or muon, and differ-

ent flavor, electron and muon, subsamples. Both experiments divide the data into events with zero, one, or two or more jets. The primary backgrounds are SM direct diboson production,  $W + \text{jets}$ , Drell-Yan, single top, and  $t\bar{t}$ . The  $t\bar{t}$  background is dominant and the division by jet counting is designed to isolate the lower jet categories which have smaller top contributions. In addition  $b$ -tag vetoes are applied including, at CMS, the vetoing of jets under a jet transverse momentum threshold. The two experiments apply additional selection criteria to further take advantage of the collinear nature of the charged leptons in Higgs boson decay to  $W$  bosons. In the two jet analysis the jets are required to have a large rapidity difference and large jet-jet invariant mass to be consistent with the forward jets from vector boson fusion.

Both experiments construct orthogonal control regions to study background kinematics and normalize background contributions. To study  $t\bar{t}$  and  $tW$  backgrounds a region is constructed with no jet multiplicity selection (ATLAS), or requiring one  $b$  tagged jet above threshold (CMS). For zero jet events the background is normalized from this region by extrapolating to the zero jet topology using top event kinematics from simulation. For events with jets the background is normalized in these regions by applying  $b$ -tagging and  $b$  mistagging rates measured in a  $t\bar{t}$  dominated region to calculate the number of top events that fail the  $b$ -tagging criteria in the data. In addition the region with one  $b$ -tagged jet can be used to study the performance of under-threshold  $b$  jets to cross-check the performance of the veto on  $b$ -tagged under-threshold jets that is used in zero jet events used in CMS. A region with diepton invariant mass larger than 80 GeV (ATLAS) or 100 GeV (CMS) is used to normalize the  $WW$  contribution. In ATLAS the contribution of Drell-Yan events produced off the  $Z$  resonance is estimated using simulation after additional selection on  $\cancel{E}_T$  and the transverse momentum of the dilepton system to reduce this contribution. In CMS, this background is estimated by measuring the  $Z$  resonance rate, subtracting non-Drell-Yan contributions using  $\mu e$  events, and then extrapolating the result to the off  $Z$  resonance mass range using the expected distribution of the dilepton mass from simulation.  $W + \text{jets}$  backgrounds are estimated using a fully data driven method relying on identifying a sample of  $W + \text{jets}$  events with a second lepton candidate passing a loose plus antilepton selection (ATLAS), or simply a loose selection (CMS), and applying false lepton identification rates measured from data.

The ATLAS experiment uses the transverse mass of the Higgs boson to search for the signal, as shown in Fig. 13, while CMS uses a BDT algorithm to distinguish signal from background.

These analyses extend the sensitivity of the searches for pairs of vector bosons to lower masses including sensitivity to masses as low as 125 GeV. The experiments exclude the ranges greater than 137 GeV (ATLAS) and 129-520 GeV (CMS). No upper limit is placed in the ATLAS analysis as the analysis was optimized for low Higgs

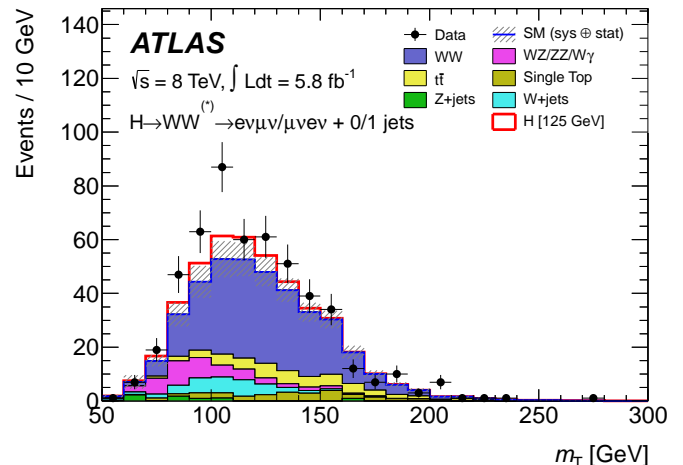


FIG. 13: Distribution of the transverse mass in the zero-jet and one-jet  $WW$  analyses of ATLAS, with both  $e\mu$  and  $\mu e$  channels combined. The expected signal for  $m_H = 125$  GeV is shown stacked on top of the background prediction.

boson mass values. Both experiments have the sensitivity to exclude a Higgs boson at smaller masses but observe an excess around  $\simeq 125$  GeV. The ATLAS excess has a local significance of  $2.8 \sigma$  and corresponds to a signal strength of  $1.4 \pm 0.5$  times the expected SM rate assuming a Higgs boson mass of 125 GeV. The CMS experiment sees a small excess with a local significance of  $1.6 \sigma$ .

#### E. Searches in $H \rightarrow WW, ZZ$ with decays of one boson to quarks or neutrinos

The ATLAS and CMS experiments conduct inclusive searches for the Higgs boson in the decay modes  $H \rightarrow W^+W^- \rightarrow \ell^+\nu q\bar{q}$  [181–183],  $H \rightarrow ZZ \rightarrow \ell^+\ell^-q\bar{q}$  [184, 185] and  $H \rightarrow ZZ \rightarrow \ell^+\ell^-\nu\bar{\nu}$  [186–188]. Although these search modes have higher backgrounds than those of the other decay modes to pairs of vector bosons discussed earlier they have strong sensitivity for high-mass Higgs bosons where the vector bosons have high transverse momentum leading to significantly reduced backgrounds.

Data are collected on one and two lepton triggers for the analyses with  $W$  and  $Z$  bosons, respectively. The charged leptons are required to pass transverse momentum and identification requirements. In the modes with  $Z \rightarrow \ell^+\ell^-$  decays the invariant mass of the charged leptons are required to be consistent with the  $Z$  boson mass while in the  $W \rightarrow \ell\nu$  case the transverse mass formed from the  $\cancel{E}_T$  and the lepton momentum is required to be consistent with the expected  $W$  boson transverse mass. In the cases where a  $Z$  boson decays to neutrinos the  $\cancel{E}_T$  is required to be large. The ATLAS experiment further divides this analysis into high and low Higgs boson mass versions where the  $\cancel{E}_T$  is required to be larger in the high-mass version. Finally, in the cases where the

vector bosons decay to quarks the jet-jet invariant mass is required to be consistent with the expectation for a  $W$  or  $Z$  boson.

The primary backgrounds are from SM diboson production,  $t\bar{t}$  production, and QCD multijet production where mismeasurement of a jet mimics one of the leptonic signatures. In all of these background processes the candidate diboson pair is not expected to form a mass resonance, and the individual vector bosons are not expected to be boosted. The experiments apply criteria to exploit these characteristics including requirements on the boost of individual vector bosons and the opening angle between vector boson decay products. After selection they search for the Higgs boson using either the full mass reconstruction ( $H \rightarrow ZZ \rightarrow \ell^+\ell^-q\bar{q}$ ), transverse mass reconstruction ( $H \rightarrow ZZ \rightarrow \ell^+\ell^-\nu\bar{\nu}$ ) or full mass reconstruction applying a  $W$  boson mass constraint in the  $H \rightarrow W^+W^- \rightarrow \ell^+\nu q\bar{q}$  mode. The experiments search for a Higgs boson in the range 130-600 GeV, with varying lower thresholds depending on the analysis, using 4.7-5.0  $\text{fb}^{-1}$  of 7 TeV collision data per experiment, while the CMS experiment additionally includes 5.1  $\text{fb}^{-1}$  of 8 TeV collision data in the  $H \rightarrow W^+W^- \rightarrow \ell^+\nu q\bar{q}$  and  $H \rightarrow ZZ \rightarrow \ell^+\ell^-\nu\bar{\nu}$  modes. The combined results provide substantial constraints on the mass of a high-mass Higgs boson excluding masses from 230 to 600 GeV. The exclusion is dominated by the  $H \rightarrow ZZ \rightarrow \ell^+\ell^-\nu\bar{\nu}$  mode although extended in the lower mass range by the  $H \rightarrow W^+W^- \rightarrow \ell^+\nu q\bar{q}$  search.

## VIII. LHC SEARCHES IN FERMIONIC HIGGS BOSON DECAYS

### A. Searches in $H \rightarrow \tau^+\tau^-$

The LHC experiments search for the SM Higgs boson in the tau lepton pair decay mode [189–191]. The Higgs boson to  $\tau$  lepton pair branching ratio is 8% to 1.5% in the Higgs boson mass range of 115-150 GeV, and  $\tau$  lepton signals are distinct enough to make this a viable search mode for all Higgs boson production processes. However, the production mode with strongest sensitivity is the vector boson fusion production mode with two associated forward jets. This mode is of high interest since observation of Higgs boson production via vector boson fusion gives direct information on how the Higgs boson interacts with high-energy longitudinal vector bosons. In addition it will allow the measurement of the coupling of the  $\tau$  lepton to the Higgs boson which should be the first mode to establish a clear signal in a fermionic decay at the LHC and is the only accessible leptonic coupling in the hadron collider environment, prior to the planned luminosity upgrades. The  $\tau\tau$  invariant mass obtained in the CMS vector boson analysis is shown in Fig. 14

The experiments search for events with zero, one, or two associated jets and oppositely charged  $\tau$  lepton pairs in the following  $\tau\tau$  decay final states:  $ee$  (ATLAS),  $\mu\mu$ ,

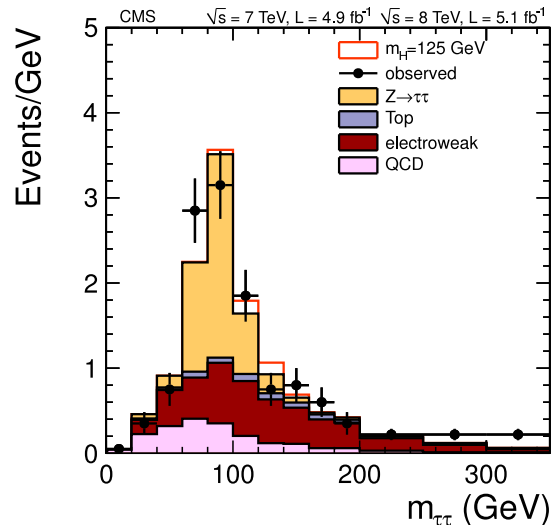


FIG. 14: Distribution of the  $\tau\tau$  invariant mass in the combined 7 and 8 TeV data sets for the VBF category of the CMS  $\tau^+\tau^-$  analysis. The expected signal for  $m_H = 125$  GeV is shown stacked on top of the background prediction.

$e\tau_h$ ,  $\mu\tau_h$ , and  $\tau_h\tau_h$  (ATLAS), where  $e$  indicates  $\tau \rightarrow e\nu\nu$ ,  $\mu$  indicates  $\tau \rightarrow \mu\nu\nu$ , and  $\tau_h$  where  $\tau_h$  indicates the  $\tau$  lepton decayed to hadrons and a  $\tau$  neutrino. Data are collected on triggers that require one or two charged leptons and in the ATLAS experiment one trigger requires two high- $p_T$   $\tau_h$  candidates ( $\tau_h\tau_h$ ).

The primary backgrounds are Drell-Yan production,  $W$ +jets production, where one jet is misidentified as a  $\tau$  lepton, and  $t\bar{t}$  production. To enhance the presence of a possible signal relative to backgrounds, the leptons or sum of hadronic decay products are required to have substantial transverse energy and the  $\cancel{E}_T$  from undetected neutrinos is required to be collinear with the direction of the dilepton system. In events with two jets, the two jets are required to have high momentum and be contained within the forward calorimeters. There also must be a large rapidity gap between the two jets consistent with the vector boson fusion hypothesis. In events with one jet, the  $p_T$  of the jet is required to be high to enhance the Higgs boson candidate boost, which improves separation of the Higgs boson signal from backgrounds and allows for a more precise estimate of the Higgs boson mass.

The experiments search for the presence of a Higgs boson using methods designed to more fully reconstruct the mass of the Higgs boson by including the  $\cancel{E}_T$  in the calculation and taking advantage of the boosted configurations. The ATLAS (CMS) experiments search for a Higgs boson in the range 110-150 GeV (110-145 GeV) using 4.7-4.9  $\text{fb}^{-1}$  of 7 TeV collision data per experiment, while the CMS experiment additionally includes 5.1  $\text{fb}^{-1}$  of 8 TeV collision data. The ATLAS experiment reaches sensitivity to set limits in the range 3-11 times the expected SM production rate, while the CMS experiment reaches sensitivities of 1.3-2.4 times the SM rate. At a

mass of 125 GeV the CMS experiment sets a limit on the Higgs boson production cross section of a SM Higgs boson of 1.1 times the expected SM rate. The sensitivity of this analysis is sufficient to achieve evidence for this decay mode using tens of  $\text{fb}^{-1}$ .

### B. Searches in $H \rightarrow b\bar{b}$

The LHC experiments conduct searches for associated production of Higgs bosons with a  $W$  or a  $Z$  boson with subsequent decay of the Higgs boson to a pair of  $b$ -quarks [192–194]. The Higgs boson to  $b$ -quark pairs branching ratio is 70% to 40% in the mass range of 115–135 GeV. However, the  $b$ -quark decay signature is not distinct enough to extract the signal from the background and the leptonic decay signatures of the massive vector bosons produced in associated production are also necessary to search for the Higgs boson in this decay mode. This search is divided into three subsearches by the decay mode of the massive vector boson. The experiments search for  $WH \rightarrow \ell\nu b\bar{b}$ ,  $ZH \rightarrow \ell^+\ell^-b\bar{b}$ , and  $ZH \rightarrow \cancel{E}_T b\bar{b}$  where the  $Z$  decays to neutrinos, “observed” as  $\cancel{E}_T$ . A charged lepton ( $\ell$ ) refers to electrons and muons of both electric charges. Although this set of production and decay processes is less sensitive than those of many other Higgs boson search modes, it is important because it can eventually be used to measure the relative couplings of the Higgs boson to the  $W$  and  $Z$  bosons and uniquely measure its coupling to  $b$  quarks.

Data are collected on triggers that require a single charged lepton for events with  $W$  decays, single leptons (ATLAS  $ee$  mode), or pairs of leptons for  $Z$  decays to charged leptons, and either  $\cancel{E}_T$  (ATLAS) or  $\cancel{E}_T$ +jets (CMS) for events with  $Z$  decays to neutrinos.

Backgrounds such as  $W$ +jets, single top and  $t\bar{t}$ , dibosons, and QCD multijet production with misidentified leptons are several orders of magnitude larger than the signal. To reconstruct a possible signal the analyses make several additional requirements. Leptons must be fully reconstructed by both the tracking system and dedicated lepton identification systems and pass minimum transverse momentum thresholds. Missing transverse momentum must not be collinear with the jets. In addition, the ATLAS experiment requires that  $\cancel{E}_T$  reconstructed using calorimeter and tracking-based algorithms is consistent, while the CMS experiment uses particle flow-based objects to take advantage of all detector subsystems. Two jets must be identified as  $b$  jets, as expected from the  $b$ -quarks from the Higgs boson decay.

Finally in the  $ZH \rightarrow \cancel{E}_T b\bar{b}$  mode the  $\cancel{E}_T$  is required to be very large. The ATLAS experiment separates the analysis into separate channels for different ranges of vector boson  $p_T$ , while the CMS experiment selects events based on the transverse momenta of both the vector and Higgs boson candidates.

The ATLAS experiment uses the invariant mass of the two  $b$  jets to search for Higgs boson candidates within

each channel, and combines the results into a single search. The CMS experiment uses variables associated with the above quantities and the dijet invariant mass of the Higgs boson as inputs to multivariate discriminants used to distinguish signal from background. The ATLAS (CMS) experiment search for a Higgs boson in the range 110–130 GeV (100–135 GeV) using  $4.7$ – $5.0 \text{ fb}^{-1}$  of 7 TeV collision data per experiment, while the CMS experiment additionally includes  $5.1 \text{ fb}^{-1}$  of 8 TeV collision data. The CMS analyses have sensitivity to set limits on the order of 1 to 5 times the expected SM Higgs boson cross section, depending on the mass, achieving a sensitivity of 1.6 at a Higgs boson mass of 125 GeV. The sensitivity of this analysis is sufficient to achieve evidence for this decay mode using tens of  $\text{fb}^{-1}$ .

### C. Searches for $t\bar{t}H$ production

The LHC experiments search for associated production of the Higgs boson with  $t\bar{t}$  where the Higgs boson is radiated from one of the top quarks. The strong coupling between the Higgs boson and the top quark increases the probability of such radiation. This process provides a direct measurement of the top-quark Yukawa coupling, which is expected to be one indicating maximal coupling. Statistically it will not be as significant as measuring the coupling in gluon fusion events, which are dominated by the top loop diagram, but it will not suffer from theoretical uncertainties associated with understanding the gluon fusion loop process. The ATLAS and CMS experiments have performed an analysis with the full 7 TeV data set [195, 196] in the final states with two leptons (CMS only) and with lepton plus jets decay modes of the top quarks with Higgs boson decay to  $b\bar{b}$ . Events with 4–6 (2–6) jets and 0–4 (2–4)  $b$ -tagged jets are considered at ATLAS (CMS). The ATLAS experiment uses the  $m_{bb}$  and  $H_T$  (total energy) distributions to set limits, while the CMS experiment uses an MVA discriminant. The CMS experiment has sensitivity to set limits on the order of 3 to 9 times the expected SM Higgs boson cross section achieving a sensitivity of 4.6 at a Higgs boson mass of 125 GeV. With a data set on the order of hundreds of  $\text{fb}^{-1}$  it is possible to directly measure the top quark Yukawa coupling in this channel.

## IX. ATLAS, CMS, AND TEVATRON RESULTS

### A. Limits and combination methods

At the LHC and Tevatron limits are calculated using the modified frequentist  $CL_s$  approach. At the Tevatron, a Bayesian technique is also used. The techniques have been shown to produce similar results at the level of about 5%. To facilitate comparisons with the SM and to accommodate analyses with different degrees of sensitivity and acceptance for more than one signal production

mechanism, the limits are divided by the SM Higgs boson production cross section, as a function of Higgs boson mass, for test masses for which the experiments have performed dedicated searches in different channels. A value of the combined limit ratio  $\mathcal{R}$  which is less than or equal to 1 indicates that that particular Higgs boson mass is excluded at the 95% C.L. Expected limits are calculated both for the background only hypothesis ( $B$ ), for which only SM background contributions are present in the selected data samples, and for the signal-plus-background hypothesis. The signal-plus-background hypothesis is calculated by also including the simulated signal contribution in the limit setting procedure. The limits are generally determined using the MVA output distributions or the invariant mass distributions, together with their associated uncertainties, as discriminating inputs to the limit setting procedure.

In the  $CL_s$  approach, each hypothesis is tested by simulating the outcome of multiple pseudoexperiments. The data are assumed to be drawn from a Poisson statistical parent distribution, and each pseudo experiment result is obtained by randomly generating pseudodata using a Poisson distribution for which the mean is taken from either the background-only or signal-plus-background hypothesis. To evaluate the statistical significance of each result a negative Poisson log-likelihood ratio (LLR) test statistic is evaluated, and the outcomes are ordered in terms of their contributing statistical significance. The frequency of each outcome is used to define the shape of the resulting LLR distributions at each mass point for both the background-only and signal-plus-background hypotheses.

Systematic uncertainties in each hypothesis are accounted for by nuisance parameters which are assigned an a priori probability distribution. These parameters refer to uncertainties in the expected background contributions and, in the case of the signal-plus-background hypothesis, also uncertainties on the simulated signal contribution. The nuisance parameters are Gaussian and randomly assigned within the parent distribution for each pseudo experiment. Correlations between the uncertainties are taken into account. To minimize the impact of the nuisance parameters the profile likelihood distribution is maximized over the nuisance parameters within each pseudo experiment, once for the background-only and once for the signal-plus-background hypotheses. Each background is allowed to vary within its uncertainties by varying the nuisance parameters in the fitting procedure, while the fit is constrained to lie within the uncertainties.

The expected limits are calculated with respect to the median of the background-only LLR distribution, whereas the observed limits are quoted with respect to the single LLR value of the actual measurement. The distribution of expected limits can also be analyzed to understand  $1\sigma$  and  $2\sigma$  deviations from median.

This framework can also produce statistical results quantifying the expectation for and properties of a sig-

nal. Given the SM expectation for signal contributions, the expected  $p$ -value or probability for backgrounds to fluctuate to the statistical significance of the expected signal can be computed. Similarly, given an excess in the data, the observed  $p$ -value can be computed. Finally, in this technique the SM Higgs signal cross section is multiplied by an arbitrary factor that is fit for the likelihood minimization allowing for a measurement of the observed cross section.

## B. ATLAS and CMS results

The ATLAS and CMS experiments analyze their data using the statistical techniques described previously. Each analysis channel is analyzed separately and within each experiment the Higgs boson search results are combined [197–201]. Table III summarizes for ATLAS and CMS, the integrated luminosities, the Higgs boson mass ranges over which the searches are performed, and references to further details for each analysis. Also given are expected and observed exclusion ranges for SM Higgs boson production at 95% C.L. or for those channels which do not have sensitivity to limit the SM rate of Higgs boson production at any mass, the expected and observed limits on cross section for the SM Higgs boson with mass  $m_H = 125$  expressed as a multiplicative factor times the predicted SM rate. Depending on the mass of a hypothetical Higgs boson, the LHC experiments have the sensitivity to discover the Higgs boson in individual production and decay channels. At some masses it is possible to have observations of the Higgs boson in several channels. The combination of these results allows the experiments to achieve larger exclusion ranges over masses where no evidence for a Higgs boson signal is seen, earlier discoveries in mass ranges where several analysis channels have sensitivity, and comparison among channels to demonstrate the consistency of a possible signal with a Higgs boson hypothesis. The LHC experiments are prepared for, but have not yet produced a joint combination of these results. For the first discovery the combination of results from multiple experiments is not preferred since simultaneous observation constitutes both an observation and an independent confirmation of the result.

Over a large region of masses the LHC experiments observe no evidence for a Higgs boson. The LHC data show a consistent picture with a high-mass SM Higgs boson typically excluded by multiple channels. At high mass the ATLAS experiment excludes the production of a SM Higgs boson with masses from 131 to 559 GeV at 95% C.L. and the CMS experiment excludes a region from 128 to 600 GeV at 95% C.L., where 600 GeV is the limit of the search range. At low mass the ATLAS experiment excludes the production of a SM Higgs boson with masses from 111 to 122 GeV at 95% C.L., while the CMS experiment excludes the region from 110 to 122.5 GeV.

TABLE II: The most significant excesses seen in ATLAS and CMS results and the combined local and global significances or P values.

Topology	ATLAS Significance and Mass	CMS Significance and Mass
$H \rightarrow WW \rightarrow \ell\nu\ell\nu$	$2.8 \sigma$ 125.0 GeV	$1.6 \sigma$ 125.0 GeV
$H \rightarrow ZZ \rightarrow 4\ell$	$3.4 \sigma$ 125.0 GeV	$3.1 \sigma$ 125.6 GeV
$H \rightarrow \gamma\gamma$	$4.5 \sigma$ 126.5 GeV	$4.1 \sigma$ 125.0 GeV
Combined Significance	$5.9 \sigma$ 126.0 GeV	$5.0 \sigma$ 125.3 GeV

TABLE III: The integrated luminosity, explored mass range, 95% C.L. expected and observed limits, and references for the ATLAS and CMS analyses. For analyses without SM sensitivity the expected and observed exclusions on cross section normalized to the SM expectation ( $\mathcal{R}$ ) assuming  $m_H = 125$  are given. For analyses with SM sensitivity expected and excluded ranges of mass are given.

ATLAS Channels	Luminosity (7+8 TeV, fb <sup>-1</sup> )	$m_H$ range (GeV)	Expected exclusion (Range in GeV, $\mathcal{R}$ )	Observed exclusion (Range in GeV, $\mathcal{R}$ )	Reference
$ttH \rightarrow t\bar{t}b\bar{b}$	4.7	110-130	–	–	[195]
$VH \rightarrow Vb\bar{b}$	4.7	110-130	$\mathcal{R} = 4.0$	$\mathcal{R} = 4.6$	[192]
$H \rightarrow \tau^+\tau^-$	4.7	100-150	$\mathcal{R} = 3.3$	$\mathcal{R} = 3.4$	[189]
$H \rightarrow \gamma\gamma$	4.8+5.9	110-150	110-139.5	112-122.5 & 132-143	[167, 168]
$H \rightarrow WW \rightarrow \ell\nu\ell\nu$	4.7+5.8	110-600	>124.5	>137.0	[177, 178]
$H \rightarrow WW \rightarrow \ell\nu 2\text{jet}$	4.7	300-600	–	–	[181]
$H \rightarrow ZZ \rightarrow 4\ell$	4.8+5.8	110-600	124-164 & 176-500	131-162 & 170-460	[171, 172]
$H \rightarrow ZZ \rightarrow 2\ell 2\text{jet}$	4.7	200-600	351-404	300-322 & 353-410	[184]
$H \rightarrow ZZ \rightarrow 2\ell 2\nu$	4.7	200-600	280-497	319-558	[186]
ATLAS Combined	4.7+5.8	110-600	110-582	111-122 & 131-559	[199]

CMS Channels	Luminosity (7+8 TeV, fb <sup>-1</sup> )	$m_H$ range (GeV)	Expected exclusion (range in GeV, $\mathcal{R}$ )	Observed exclusion (range in GeV, $\mathcal{R}$ )	Reference
$ttH \rightarrow t\bar{t}b\bar{b}$	5.0	110-130	$\mathcal{R} = 4.6$	$\mathcal{R} = 3.8$	[196]
$VH \rightarrow Vb\bar{b}$	5.0+5.1	110-135	$\mathcal{R} = 1.6$	$\mathcal{R} = 2.1$	[193, 194]
$H \rightarrow \tau^+\tau^-$	4.9+5.1	110-145	$\mathcal{R} = 1.28$	$\mathcal{R} = 1.06$	[190, 191]
$H \rightarrow \gamma\gamma$	5.1+5.3	110-150	110-144	–	[169, 170]
$H \rightarrow WW \rightarrow \ell\nu\ell\nu$	4.9+5.0	120-600	122-450	129-520	[179, 180]
$H \rightarrow WW \rightarrow \ell\nu 2\text{jet}$	5.0+5.1	170-600	220-515	230-480	[182, 183]
$H \rightarrow ZZ \rightarrow 4\ell$	5.1+5.3	110-600	121-570	131-162 & 172-525	[173, 174]
$H \rightarrow ZZ \rightarrow 2\ell 2\tau$	4.6	190-600	–	–	[175]
$H \rightarrow ZZ \rightarrow 2\ell 2\text{jet}$	4.6	130-600	–	–	[185]
$H \rightarrow ZZ \rightarrow 2\ell 2\nu$	5.0+5.0	200-600	290-530	278-600	[187, 188]
CMS Combined	5.1+5.3	110-600	110-600	110-122.5 & 127-600	[201]

The combined ATLAS and CMS limits are presented in Figs. 15 and 16, respectively.

At low masses the experiments have the sensitivity to exclude or observe the Higgs boson. The sensitivities for observation of a signal are quantified as an expected  $p$ -value for the background to fluctuate to a signal as large as the median expectation for a SM Higgs boson. The combined expected  $p$ -value at  $m_H = 125$  GeV is  $4.9 \sigma$  for the ATLAS experiment and  $5.8 \sigma$  for the CMS experiment. In the region around 125 GeV both experiments observe an excess of events in multiple search channels. The experiments evaluate the  $p$  values for each channel separately and for the entire combination and compare those values with the expected background-only  $p$  values given a SM Higgs boson as a function of mass (see Fig. 17,18). Information quantifying the most signifi-

cant excesses in the individual search channels was given previously in the sections describing the different LHC Higgs boson searches and is summarized along with the most significant combined excess from each experiment in Table II. Both experiments observe a Higgs boson signal with local significances above the evidence level of  $3 \sigma$  in the  $ZZ$  and  $\gamma\gamma$  decay modes and combined significances of  $5.9 \sigma$  at  $m_H = 126$  GeV for the ATLAS experiment and  $5.0 \sigma$  at  $m_H = 125.3$  for the CMS experiment. The ATLAS experiment also evaluates a global significance over their entire search range assuming no a priori knowledge of the SM Higgs boson and finds a global significance of  $5.1 \sigma$ . The simultaneous observation of a new particle with mass of approximately 125 GeV constitutes a definitive discovery. The decay modes in which the particle is strongly observed also indicate that the



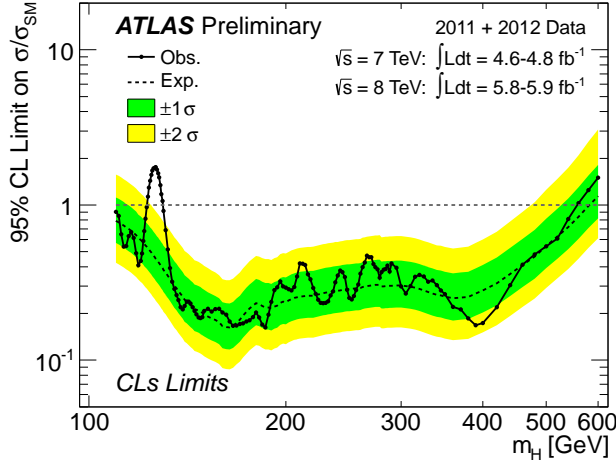


FIG. 15: The ATLAS experiments combined upper limit as a function of the Higgs boson mass between 100 and 600 GeV. Solid black: observed limit/SM; dashed black: median expected limit/SM in the background-only hypothesis; colored bands:  $\pm 1, 2\sigma$  distributions around the median expected limit.

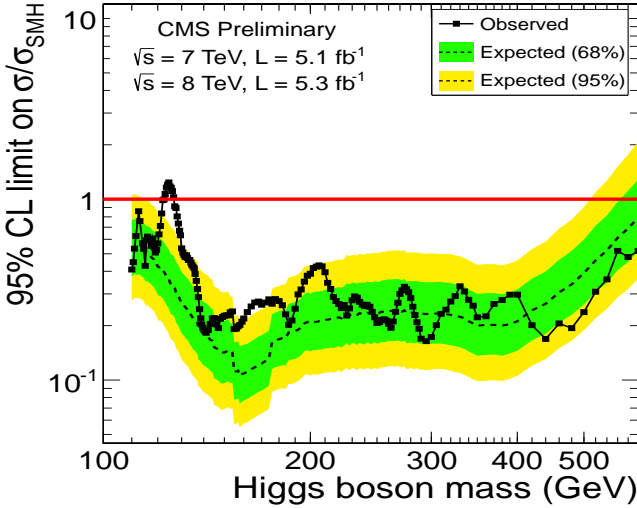


FIG. 16: The CMS experiments combined upper limit as a function of the Higgs boson mass between 100 and 600 GeV. Solid black: observed limit/SM; dashed black: CMS expected limit/SM in the background-only hypothesis; colored bands:  $\pm 1, 2\sigma$  distributions around the median expected limit.

particle is a boson and plays a role in the mechanism of electroweak symmetry breaking.

The CMS and ATLAS Collaborations measured several properties to understand the compatibility of the observed boson with the SM Higgs boson and present the results in their papers reporting the observations [199, 201].

The experiments fit for the cross section for Higgs boson production given the observed data in each decay channel and globally combining all decay channels. The

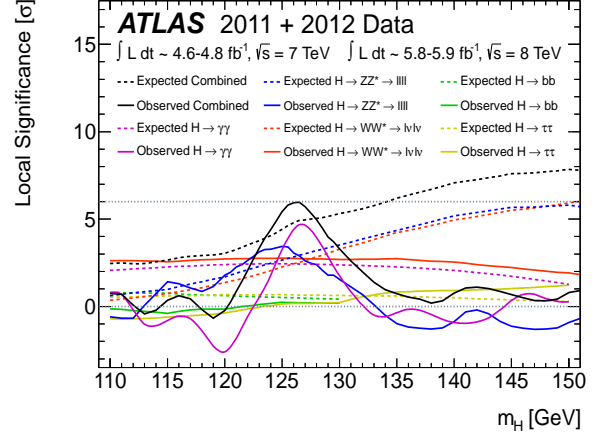


FIG. 17: ATLAS local significance [199] for each search channel and the combination. The observed significance are shown with solid curves, and the median expected significance assuming a signal is present at the SM strength are shown with dashed curves. A dash-dotted line indicates the  $6\sigma$  threshold. The highest local significances of the  $ZZ$  and  $\gamma\gamma$  channels are  $3.4\sigma$  and  $4.5\sigma$  respectively while the combined significance of all channels is  $5.9\sigma$ .

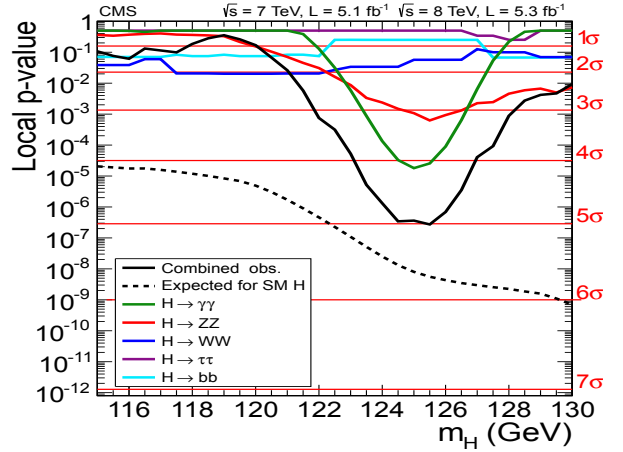


FIG. 18: CMS local  $p$  values [201]. The observed  $p$  values are shown with solid curves, and the median expected  $p$  value for the combined search assuming a signal is present at the SM strength is shown with a dashed curve. Horizontal lines indicate the  $1\sigma - 7\sigma$  thresholds. The highest local significances of the  $ZZ$  and  $\gamma\gamma$  channels are  $3.1\sigma$  and  $4.1\sigma$  respectively while the combined significance of all channels is  $5.1\sigma$ .

results are presented as a ratio to the expected SM values in Figs. 19 and 20 for the ATLAS and CMS experiments, respectively. Of note are the larger than expected cross-section times branching ratios seen in the  $\gamma\gamma$  (ATLAS and CMS) and  $ZZ$  (ATLAS) decay modes. These modes are dominated by gluon fusion production. The combined signal strengths measured by the experiments are  $1.4 \pm 0.3$  for ATLAS and  $0.87 \pm 0.23$  for CMS compatible with the SM Higgs boson expectation. Individual signal

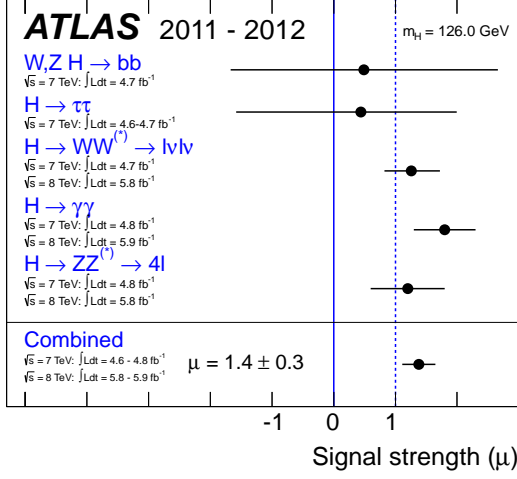


FIG. 19: ATLAS best-fit signal strength for all SM Higgs boson decays for  $m_H = 125 \text{ GeV}/c^2$ .

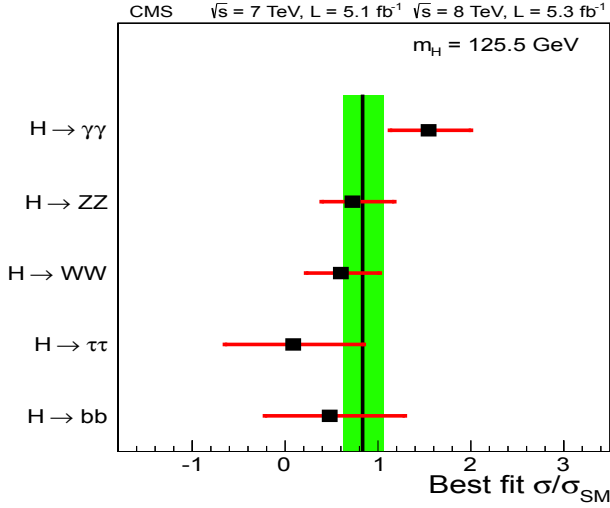


FIG. 20: CMS best-fit signal strength for all SM Higgs boson decays for  $m_H = 125 \text{ GeV}/c^2$ . Untagged refers to the cross section extracted from topologies sensitive to gluon fusion production. The shaded band corresponds to the  $\pm 1\sigma$  uncertainty on the full combination.

strengths in the most sensitive modes were discussed in the sections on individual searches.

The fully reconstructed decays of the Higgs boson  $H \rightarrow \gamma\gamma$  and  $H \rightarrow ZZ \rightarrow \ell^+\ell^-\ell^+\ell^-$  have excellent mass resolution. The  $H \rightarrow W^+W^- \rightarrow \ell^+\nu\ell^-\bar{\nu}$  decay mode has substantial rate but has poor mass resolution due to the two neutrinos in the final state. The ATLAS experiment measures a mass for the observed boson of  $m_H = 126.0 \pm 0.4(stat) \pm 0.4(sys) \text{ GeV}$  using all three decay modes. The individual fits in a two-dimensional

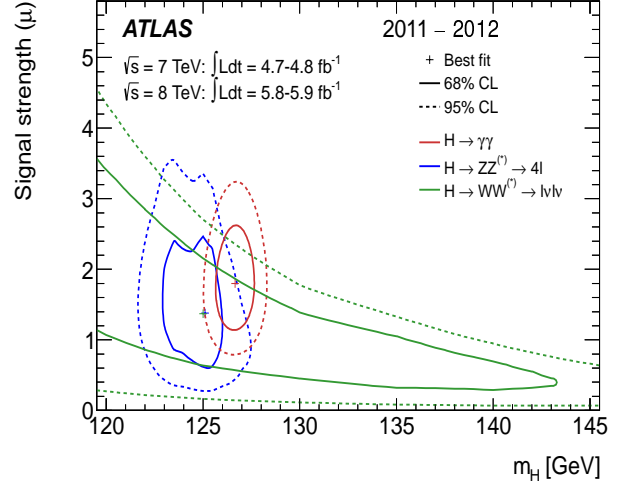


FIG. 21: The ATLAS two dimensional fit for the cross section and compared to the SM expectation and the Higgs boson mass for highest significance decay channels.

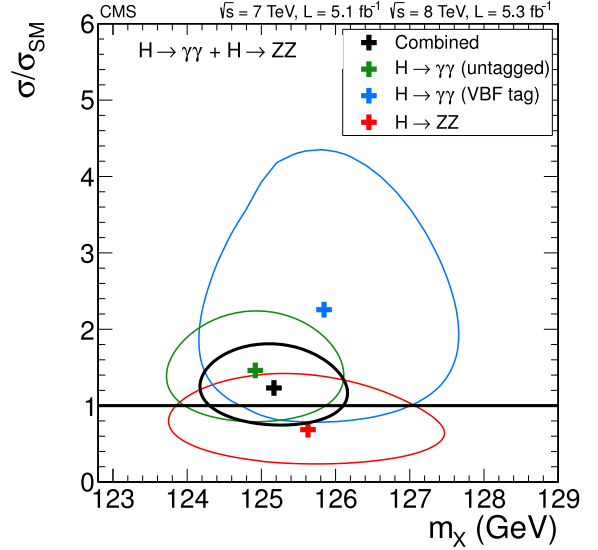


FIG. 22: The CMS two dimensional fit for the cross section and compared to the SM expectation and the Higgs boson mass for highest significance decay channels and the combined fit using those channels.

analysis of signal strength versus mass are shown in Fig. 21. The CMS experiment uses the fully reconstructed  $H \rightarrow \gamma\gamma$  and  $H \rightarrow ZZ \rightarrow \ell^+\ell^-\ell^+\ell^-$  modes to measure a mass of  $m = 125.3 \pm 0.4(stat) \pm 0.5(sys) \text{ GeV}$ . The individual and combined fits are shown in Fig. 22. The results are compatible with limits from previous searches and the prediction of the SM Higgs boson mass from constraints derived from electroweak measurements.

If the observed boson is involved in the mechanism of electroweak symmetry breaking, the measurement of its coupling to the  $W$  and  $Z$  bosons is a crucial discrimi-

nant. The production and decay rates measured by the experiments are compatible with the SM. The ratio of the  $W$  and  $Z$  couplings can be computed by dividing the production times decay rates for  $H \rightarrow WW$  and  $H \rightarrow ZZ$  since the production of the Higgs boson takes place via the same mechanisms. The ATLAS experiment measures  $R_{WZ} = 1.07^{+0.35}_{-0.27}$  [202] and the CMS experiment measures  $R_{WZ} = 0.9^{+1.1}_{-0.6}$  consistent with the SM expectation where both experiments have normalized the measurement so that the expected value in the SM is 1.

In summary, the LHC experiments extended the LEP exclusion to 122.5 GeV and further excluded a SM Higgs boson with mass between 128 and 600 GeV. The ATLAS and CMS experiments both observe a significant excess of events in the region around 125 GeV with evidence for the production of a new boson in the  $ZZ$  and  $\gamma\gamma$  decay modes, with observed local significances of  $4.5\sigma$  and  $4.1\sigma$  in the  $\gamma\gamma$  mode and  $3.4\sigma$  and  $3.1\sigma$  in the  $ZZ$  mode. Significant signals ( $2.8\sigma$  and  $1.6\sigma$ ) are also observed in the  $H \rightarrow WW$  decay mode, while the observed significance in the fermionic modes ( $H \rightarrow \tau\tau$  and  $H \rightarrow b\bar{b}$ ) is weak, which is not unexpected given the currently low expected significance in these modes. When combining all their channels, both experiments independently report the discovery of a new boson and provide first measurements of its fundamental properties, in agreement with those expected from a SM Higgs boson with a mass close to 125 GeV.

### C. Tevatron combined results

As in the LHC experiments, to simplify the combination, the searches are separated into mutually exclusive final states. Table IV summarizes for each CDF and D0 search the integrated luminosities, the Higgs boson mass ranges over which the searches are performed, the ratios of expected and observed limits with respect to SM Higgs boson expectations achieved for  $m_H = 125$  GeV, and the references to further details for each analysis. Using the combination procedure outlined in Sec. IX B, limits on SM Higgs boson production  $\sigma \times B(H \rightarrow X)$  in  $p\bar{p}$  collisions at  $\sqrt{s} = 1.96$  TeV for  $100 \leq m_H \leq 200$  GeV are extracted.

The combinations of results from each single experiment [203, 204], as used in this Tevatron combination, yield the following ratios of 95% C.L. observed (expected) limits to the SM expectation: 2.4 (1.2) for CDF and 2.2 (1.6) for D0 at  $m_H = 115$  GeV, 2.9 (1.4) for CDF and 2.5 (1.9) for D0 at  $m_H = 125$  GeV, and 0.42 (0.69) for CDF and 0.94 (0.76) for D0 at  $m_H = 165$  GeV.

The ratios of the 95% C.L. expected and observed limits to the SM cross section are shown in Fig. 23 for the combined CDF and D0 analyses. The observed (expected) limit values are 1.8 (0.94) at  $m_H = 115$  GeV, 2.2 (1.1) at  $m_H = 125$  GeV, and 0.39 (0.49) at  $m_H = 165$  GeV.

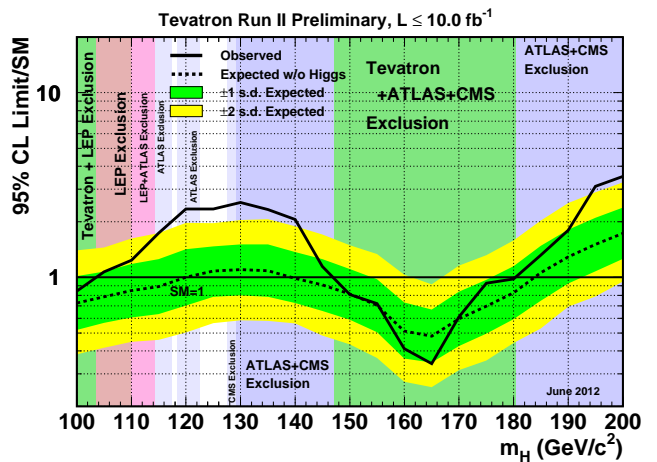


FIG. 23: Observed and expected 95% C.L. upper limits on the ratios to the SM cross section, as functions of the Higgs boson mass for the combined CDF and D0 analyses. The bands indicate the 68% and 95% probability regions where the limits can fluctuate, in the absence of signal.

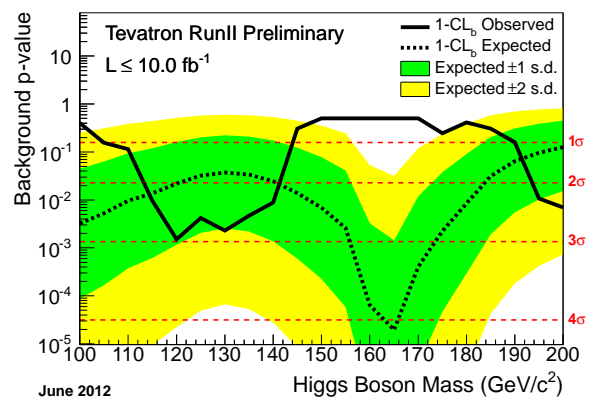


FIG. 24: The background  $p$  values  $1-CL_b$  as a function of the Higgs boson mass (in steps of 5 GeV), for the combination of the CDF and D0 analyses. The green and yellow bands correspond, respectively, to the regions enclosing  $1\sigma$  and  $2\sigma$  fluctuations around the median prediction in the signal-plus-background hypothesis at each value of  $m_H$ .

Fig. 24 shows the  $p$  value  $1-CL_b$  as a function of  $m_H$ , i.e., the probability that an upward fluctuation of the background can give an outcome as signal-like as the data or more. In the absence of signal, the  $p$  value is expected to be uniformly distributed between 0 and 1. A small  $p$  value indicates that the data are unlikely to be explained by the background-only hypothesis. The smallest observed  $p$  value corresponds to a Higgs boson mass of 120 GeV and has a local significance of  $3.0\sigma$ . The fluctuations seen in the observed  $p$  value as a function of the tested  $m_H$  result from excesses seen in different

TABLE IV: The integrated luminosity, explored mass range, 95% C.L. expected and observed limits on Higgs boson production cross section relative to the SM expectation ( $\mathcal{R}$ ) assuming  $m_H = 125$  GeV, and references for the different CDF and D0 analyses grouped by the final states ( $\ell = e$  or  $\mu$ ) considered.

CDF Channels	Luminosity ( $\text{fb}^{-1}$ )	$m_H$ range (GeV)	exp. $\mathcal{R}$	obs. $\mathcal{R}$	Reference
			125 GeV	125 GeV	
$WH \rightarrow \ell\nu b\bar{b}$ 2-jet & 3jet channels	9.5	100–150	2.8	4.9	[113]
$ZH \rightarrow \ell^+\ell^- b\bar{b}$ 2-jet & 3 jet channels	9.5	100–150	3.6	7.2	[117]
$ZH \rightarrow \nu\bar{\nu} b\bar{b}$ 2-jet & 3jet channels	9.5	100–150	3.6	6.8	[121]
$H \rightarrow W^+W^-$ & $WH \rightarrow WW^+W^-$ & $ZH \rightarrow ZW^+W^-$	9.7	110–200	3.1	3.0	[145]
$H \rightarrow \gamma\gamma$	10.0	100–150	9.9	17.0	[129]
$H \rightarrow ZZ$ (four leptons, limits are given at 130 GeV)	9.7	120–200	18.3	20.5	[151]
$H \rightarrow W^+W^- (e\tau_h) + (\mu\tau_h)$ & $WH \rightarrow WW^+W^- (1\tau_h)$	9.7	130–200	.	.	[150]
$H + X \rightarrow \tau^+\tau^- (1\text{ jet}) + (2\text{ jet})$	8.3	100–150	14.8	11.7	[125]
$WH \rightarrow \ell\nu\tau^+\tau^- / ZH \rightarrow \ell^+\ell^-\tau^+\tau^-$	6.2	100–150	23.3	26.5	[126]
$WH + ZH \rightarrow jjb\bar{b}$ (SS,SJ)	9.5	100–150	9.0	11.0	[107]
$t\bar{t}H \rightarrow WWb\bar{b}b\bar{b}$ (no lepton) - (lepton)	5.7-9.5	100–150	12.4	17.6	[131, 132]

D0 Channels	Luminosity ( $\text{fb}^{-1}$ )	$m_H$ range (GeV)	exp. $\mathcal{R}$	obs. $\mathcal{R}$	Reference
			125 GeV	125 GeV	
$WH \rightarrow \ell\nu b\bar{b}$ 2-jet & 3jet channels	9.7	100–150	4.7	5.2	[114]
$ZH \rightarrow \ell^+\ell^- b\bar{b}$ 2-jet & 3jet channels	9.7	100–150	5.1	7.1	[118]
$ZH \rightarrow \nu\bar{\nu} b\bar{b}$ 2-jet channel	9.5	100–150	3.9	4.3	[122]
$H \rightarrow W^+W^- \rightarrow \ell^\pm\nu\ell^\mp\nu$	8.6-9.7	115–200	3.6	4.6	[146]
$H \rightarrow \gamma\gamma$	9.7	100–150	8.2	12.9	[130]
$H \rightarrow W^+W^- \rightarrow \mu\nu\tau_h\nu$	7.3	115–200	12.8	15.7	[127]
$H \rightarrow W^+W^- \rightarrow \ell\nu jj$	5.4	130–200	.	.	[149]
$H + X \rightarrow \ell^\pm\tau_h^\mp jj$	4.3-6.2	105–200	40.0	44.0	[127]
$VH \rightarrow \tau\tau\mu + X$	7.0	115–200	17.6	13.1	[128]
$VH \rightarrow e^\pm\mu^\pm + X$	9.7	115–200	11.6	7.8	[147]
$VH \rightarrow \ell\ell\ell + X$	9.7	100–200	11.1	19.3	[148]

search channels, as well as from point-to-point fluctuations originating from the separate discriminants used at each  $m_H$ , as next discussed in more detail. The width of the dip from 115 to 135 GeV is consistent with the combined resolution of the  $H \rightarrow b\bar{b}$  and  $H \rightarrow W^+W^-$  channels. The effective resolution of this search comes from two independent sources.: the reconstructed candidate masses, which directly constrain  $m_H$ , and the expected cross sections times the relevant branching ratios for the  $H \rightarrow b\bar{b}$  and  $H \rightarrow W^+W^-$  channels, which are functions of  $m_H$  in the SM. The observed excess in the  $H \rightarrow b\bar{b}$  channels coupled with a less signal-like outcome in the  $H \rightarrow W^+W^-$  channels determines the shape of the observed  $p$  value as a function of  $m_H$ .

The strongest sensitivity at low mass comes from the  $H \rightarrow b\bar{b}$  channels. The largest local significance in the combination of  $H \rightarrow b\bar{b}$  channels is  $3.3\sigma$  at a mass of 135 GeV, while it is  $2.8\sigma$  at 125 GeV [108].

In Fig. 25, the signal strength is allowed to vary as a function of  $m_H$  in the fit of the signal-plus-background hypothesis to the observed data over the full mass range. As shown, the resulting best-fit signal strength normalized to the SM prediction is within  $1\sigma$  of the SM expectation for a Higgs boson signal in the range  $110 < m_H < 140$  GeV. The largest signal fit in this range, nor-

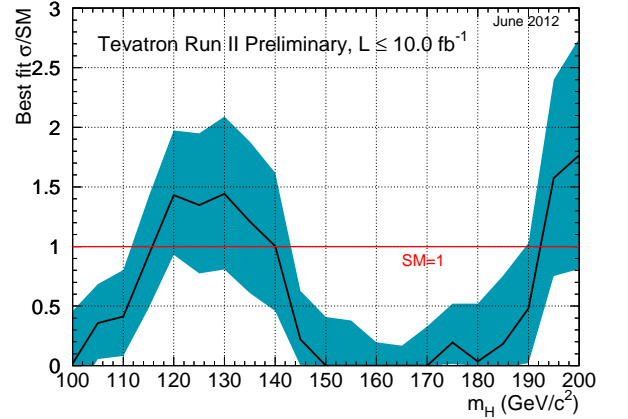


FIG. 25: The best-fit signal cross section of all CDF and D0 search channels combined shown as a ratio to the SM cross section as a function of the tested Higgs boson mass. The horizontal line at 1 represents the signal strength expected for a SM Higgs boson hypothesis. The blue band shows the  $1\sigma$  uncertainty on the signal fit.

malized to the SM prediction, is obtained at 130 GeV, rather than for the smallest  $p$ -value mass of 120 GeV,

since the similar excesses for these two mass hypotheses translate into a higher signal strength at 130 GeV. The excess in signal-strength around 200 GeV occurs in a region of low expected sensitivity ( $\sim 1 \sigma$ ) and with an unphysically narrow mass range; thus it cannot be attributed to a SM Higgs boson signal at high mass.

At the Tevatron the look-elsewhere effect (LEE) is estimated in a simplified and conservative manner. In the mass range 115–150 GeV, where the low-mass  $H \rightarrow b\bar{b}$  searches dominate, the reconstructed mass resolution is approximately 15%. A LEE factor of  $\simeq 2$  is thus estimated for the low-mass region. The  $H \rightarrow \gamma\gamma$  searches have a much better mass resolution, of the order of 3%, but their contribution to the final LLR is small due to the much smaller signal-to-background ratio in those searches. The  $H \rightarrow \tau^+\tau^-$  searches have both worse reconstructed mass resolution and lower signal to background ratio than the  $H \rightarrow b\bar{b}$  searches, and therefore similarly do not play a significant role in the estimation of the LEE. The  $H \rightarrow WW$  channel has the poorest mass resolution and therefore contributes weakly to the LEE. For the combined search of all Tevatron channels, with a conservative LEE of  $\simeq 4$  to take into account the full range over which the search was performed, the global significance of the excess observed at low mass is approximately  $2.5 \sigma$

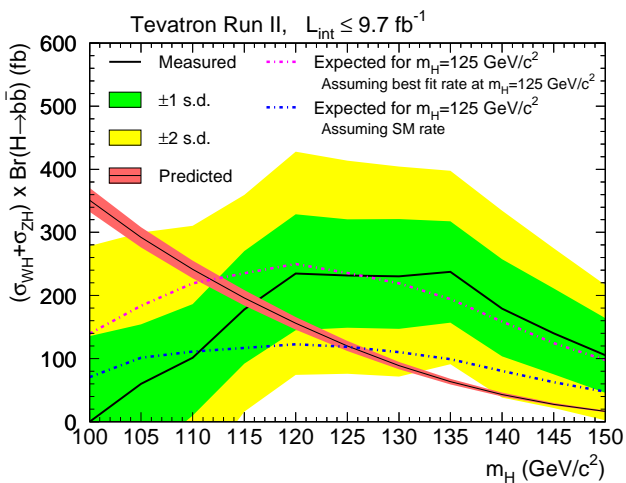


FIG. 26: The best-fit cross section times branching ratio  $\sigma_{WH} + \sigma_{ZH} \times \mathcal{B}(H \rightarrow b\bar{b})$  as a function of  $m_H$  measured at the Tevatron.

Applying the low-mass LEE to the most significant local  $p$  value obtained from the CDF+D0  $H \rightarrow b\bar{b}$  combination, a global significance of approximately  $3.1 \sigma$  is obtained, resulting in evidence for the production of a resonance in the  $b$ -flavored dijet mass distribution, produced in association with a massive vector boson. Given the mass resolution in this final state, this resonance is consistent with the new boson observed by the LHC experiments, and provides the first evidence for fermionic decays of this boson.

The measured cross section times branching ratio

$\sigma_{WH} + \sigma_{ZH} \times \mathcal{B}(H \rightarrow b\bar{b})$  is shown in Fig. 26 as a function of  $m_H$ . The resulting value is  $0.23^{+0.09}_{-0.08}$  pb for  $m_H = 125$  GeV, consistent with the corresponding SM prediction of  $0.12 \pm 0.01$  pb. The best fit signal cross section from the combined CDF and D0 analyses separated into the different Higgs boson decay channels is shown in Fig. 27, assuming  $m_H = 125$  GeV.

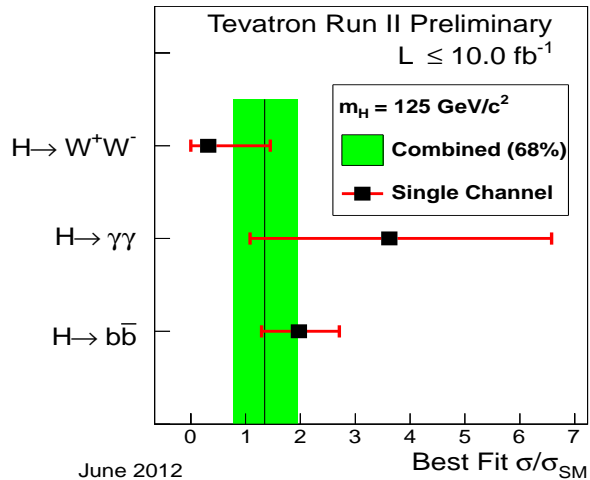


FIG. 27: Best-fit signal strength for the three most sensitive boson decay modes at the Tevatron, for  $m_H = 125$  GeV/ $c^2$ . The shaded band corresponds to the  $\pm 1 \sigma$  uncertainty on the full combination.

In summary, at the Tevatron, when combining all search channels, there is significant excess of data events with respect to the background estimation in the mass range  $115 < m_H < 135$  GeV. The  $p$  value for a background fluctuation to produce such an excess corresponds to a local significance of  $3.0 \sigma$  at 120 GeV. The largest excess is observed in the  $H \rightarrow b\bar{b}$  channels, with a local significance of  $3.3 \sigma$ , which results in a global significance of  $\approx 3.1 \sigma$  when accounting for look-elsewhere effects. The CDF and D0 Collaborations thus report evidence for the production of a resonance in the  $b$ -flavored dijet mass distribution produced in association with a massive vector boson, consistent with the new boson observed by the LHC Collaborations. The measured cross section for this process is consistent with the cross section expected for a SM Higgs boson of 125 GeV produced in association with a  $W$  or a  $Z$  boson.

#### D. Conclusion and prospects

The LHC experiments have discovered a new boson with mass around 125 GeV and have evidence for this particle in several decay modes. The Tevatron experiments report evidence for a particle, produced in association with  $W$  or  $Z$  bosons and which decays to  $b\bar{b}$ , with a mass compatible to that reported by the LHC experiments. The production and decay modes that have

been observed indicate that this boson plays a role in the mechanism of electroweak symmetry breaking and also in the mass generation for the quarks. The properties of this boson are compatible with those expected for a SM Higgs boson but more study is required to fully explore the nature of this discovery. The discovery of a new boson with properties indicating that it plays a role in electroweak symmetry breaking is a major breakthrough in fundamental physics.

The LHC experiments expect to integrate up to  $30 \text{ fb}^{-1}$  of data at 8 TeV center of mass energy by late 2012. These data should be sufficient to make first measurements of all accessible parameters of the boson assuming

SM-like behavior. After the 2012 run the LHC is expected to undergo a long shutdown to upgrade the energy and luminosity capabilities of the accelerator, to near the design parameters of 14 TeV and  $100 \text{ fb}^{-1}$  per year. Data taken after the upgrades should allow for precision measurements of the boson's properties and exploration of non SM physics associated with the boson.

*After completion of this review, additional data taken by the ATLAS and CMS collaborations confirmed that the new discovered boson is a Higgs boson, while the current precision of its measured properties does not yet allow one to definitely identify it as the standard model Higgs boson.*

- 
- [1] P.W. Higgs, Phys. Rev. Lett. 12, 132 (1964), *idem*, Phys. Rev. 145, 1156 (1966)
- [2] F. Englert and R. Brout, Phys. Rev. Lett. 13, 321 (1964)
- [3] G.S. Guralnik, C.R. Hagen, and T.W. Kibble, Phys. Rev. Lett. 13, 585 (1964)
- [4] S.L. Glashow, Nucl. Phys. 22, 579 (1961)
- [5] S. Weinberg, Phys. Rev. Lett. 19, 1264 (1967)
- [6] A. Salam, *Elementary Particle Theory*, ed: N. Svartholm, Almqvist, and Wiksells (1968)
- [7] S.L. Glashow, J. Iliopoulos, and L. Maiani, Phys. Rev. D 2, 1285 (1970)
- [8] J.F. Gunion, H.E. Haber, G.L. Kane, and S. Dawson, *The Higgs Hunter's Guide* (Addison-Wesley) (1990)
- [9] A. Djouadi, M. Spira, P.M. Zerwas, Phys. Lett. B264, 440 (1991)
- [10] S. Dawson, Nucl. Phys. B359, 283 (1991)
- [11] R.V. Harlander and W.B. Kilgore, Phys. Rev. Lett. 88, 201801 (2002) arXiv:hep-ph/0201206
- [12] C. Anastasiou and K. Melnikov, Nucl. Phys. B646, 220 (2002) arXiv:hep-ph/0207004
- [13] V. Ravindran, J. Smith, W.L. van Neerven, Nucl. Phys. B665, 325 (2003) arXiv:hep-ph/0302135
- [14] S. Actis, G. Passarino, C. Sturm, S. Uccirati, Phys. Lett. B670, 12 (2008) arXiv:0809.1301 [hep-ph]
- [15] U. Aglietti, R. Bonciani, G. Degrassi, A. Vicini, Phys. Lett. B595, 432 (2004) arXiv:hep-ph/0404071
- [16] G. Degrassi and F. Maltoni, Phys. Lett. B600, 255 (2004) arXiv:hep-ph/0407249
- [17] C. Anastasiou, R. Boughezal and F. Petriello, JHEP 0904, 003 arXiv:0811.3458 (2009)
- [18] M. Kramer, E. Laenen and M. Spira, Nucl. Phys. B511, 523 (1998) arXiv:hep-ph/9611272
- [19] K.G. Chetyrkin, B.A. Kniehl, M. Steinhauser, Nucl. Phys. B510, 61 (1998) arXiv:hep-ph/9708255
- [20] D. de Florian, M. Grazzini and Z. Kunszt, Phys. Rev. Lett. 82, 5209 (1999)
- [21] V. Ravindran, J. Smith and W. L. Van Neerven, Nucl. Phys. B 634, 247 (2002) arXiv:0201114 [hep-ph]
- [22] S. Catani, D. de Florian, M. Grazzini, P. Nason, JHEP 0307, 028 (2003) arXiv:hep-ph/0306211
- [23] S. Moch and A. Vogt, Phys. Lett. B631, 48 (2005)
- [24] E. Laenen and L. Magnea, Phys. Lett. B632, 270 (2006) arXiv:hep-ph/0508265
- [25] A. Idilbi, X. d. Ji, J. P. Ma, F Yuan, Phys. Rev. D 73, 077501 (2006) arXiv:hep-ph/0509294
- [26] V. Ravindran, Nucl. Phys. B746, 58 (2006) arXiv:hep-ph/0512249
- [27] D. de Florian and M. Grazzini, Phys. Lett. B674, 291 (2009) arXiv:0901.2427 [hep-ph]
- [28] J. Baglio and A. Djouadi, JHEP 1103 055 (2011) arXiv:1012.0530 [hep-ph]
- [29] C. Anastasiou, S. Buehler, F. Herzog, and A. Lazopoulos, JHEP 1204 004 (2012) arXiv:1202.3638 [hep-ph]
- [30] D. de Florian, G. Ferrera, M. Grazzini, and D. Tommasini, JHEP 1111 064 (2011) arXiv:1109.2109 [hep-ph]
- [31] E. Bagnaschi, G. Degrassi, P. Slavich and A. Vicini, JHEP 1202 88 (2012) arXiv:1111.2854 [hep-ph]
- [32] C. R. Schmidt, Phys. Lett. B413,391(1997)
- [33] C.J. Glosser and C.R. Schmidt, JHEP 0212, 016(2002)
- [34] J. M. Campbell, R. K. Ellis, and G. Zanderighi, JHEP 0610, 028 (2006)
- [35] J. M. Campbell, R. K. Ellis, and C. Williams, Phys. Rev. D81,074023(2010)
- [36] K.A.Assamagan *et al.*, (2004) arXiv:hep-ph/0406152
- [37] O. Brein, A. Djouadi, R. Harlander, Phys. Lett. B579, 149 (2004) arXiv:hep-ph/0307206
- [38] M.L. Ciccolini, S. Dittmaier, M. Krämer, Phys. Rev. D68, 073003 (2003) arXiv:hep-ph/0306234
- [39] J. Baglio and A. Djouadi, J. High Energy Phys. 1010, 064 arXiv:1009.1363 (2010)
- [40] G. Ferrera, M. Grazzini and F. Tramontano, Phys. Rev. Lett. 107, 152003 arXiv:1107.1164 (2011)
- [41] A. Denner, S. Dittmaier, S. Kallweit and A. Muck, arXiv:1112.5142 [hep-ph] (2011)
- [42] O. Brein, R. Harlander, M. Wiesemann and T. Zirke (2011) arXiv:1111.0761 [hep-ph]
- [43] T. Figy, S. Palmer, G. Weiglein, JHEP 1202, 105 (2012) arXiv:1012.4789 [hep-ph]
- [44] P. Bolzoni, F. Maltoni, S.-O. Moch, M. Zaro, Phys. Rev. Lett. 105, 011801 (2010) arXiv:1003.4451 [hep-ph]
- [45] M. Ciccolini, A. Denner, S. Dittmaier, Phys. Rev. Lett. 99, 161803 (2007) arXiv:0707.0381 [hep-ph]
- [46] Ciccolini, A. Denner, S. Dittmaier, Phys. Rev. D 77, 103002 arXiv:0710.4749 [hep-ph] (2008)
- [47] T. Han, G. Valencia, S. Willenbrock, Phys. Rev. Lett. 69, 3274 arXiv:hep-ph/9206246 (1992)
- [48] E.L. Berger, J. Campbell, Phys. Rev. D 70, 073011 arXiv:hep-ph/0403194 (2004)
- [49] T. Figy, C. Oleari, D. Zeppenfeld, Phys. Rev. D 68, 073005 arXiv:hep-ph/0306109 (2003)

- [50] S. Dittmaier *et al.*, [LHC Higgs Cross Section Working Group], (2012) arXiv:1201.3084 [hep-ph]
- [51] W. Beenakker, S. Dittmaier, M. Krämer, B. Plümper, M. Spira and P.M. Zerwas, Phys. Rev. Lett. **87**, 201805 (2001) arXiv:hep-ph/0107081
- [52] L. Reina and S. Dawson, Phys. Rev. Lett. **87**, 201804 (2001)
- [53] S. Dawson, L.H. Orr, L. Reina, D. Wackerroth, Phys. Rev. D **67**, 071503 (2003) arXiv:hep-ph/0107101
- [54] W. Beenakker, S. Dittmaier, M. Krämer, B. Plümper, M. Spira and P.M. Zerwas, Nucl. Phys. B **653**, 151 (2003) arXiv:hep-ph/0211352
- [55] S. Dittmaier *et al.*, [LHC Higgs Cross Sections Working Group], (2011) arXiv:1101.0593 [hep-ph]
- [56] For a compilation of theoretical results for SM and MSSM Higgs cross sections at the LHC see: <https://twiki.cern.ch/twiki/bin/view/LHCPhysics/CrossSections>.  
For the SM Higgs production via gluon fusion using Renormalization Group improved predictions see: <http://rghiggs.hepforge.org/> (2012).
- [57] LEP Electroweak Working Group, status of March (2012), <http://lepewwg.web.cern.ch/LEPEWWG/>, The ALEPH, CDF, DØ, DELPHI, L3, OPAL, SLD Collaborations, the LEP Electroweak Working Group, the Tevatron Electroweak Working Group, and the SLD Electroweak and Heavy Flavor groups, LEPEWWG/2009-01 (2009) arXiv:0911.2604 [hep-ex] ,
- [58] J. Erler and P. Langacker, Phys.Lett. B **592** 1 (2004) arXiv:hep-ph/0407097
- [59] CDF and D0 Collaborations, and the Tevatron Electroweak Working Group, (2011) arXiv:1107.5255
- [60] Tevatron Electroweak Working Group, CDF and D0 Collaborations, (2012) arXiv:1204.0042 [hep-ex]
- [61] B.L. Ioffe and V.A. Khoze, Sov. J. Part. Nucl. Phys. **9**, 50 (1978)
- [62] J. Ellis *et al.*, Nucl. Phys. B **106**, 292 (1976)
- [63] D.R.T. Jones and S.T. Petcov, Phys. Lett. **84B**, 440 (1979)
- [64] R.N. Cahn and S. Dawson, Phys. Lett. **136B**, 196 (1984), *ibid.*, **138B**, 464 (1984)
- [65] W. Kilian, M. Krmer, P. Zerwas, Phys. Lett. B **373**, 135 (1996) arXiv:hep-ph/9512355
- [66] ALEPH, DELPHI, L3, and OPAL Collaborations, The LEP Working Group for Higgs Boson Searches, Phys. Lett. B **565**, 61 (2003) arXiv:hep-ex/0306033
- [67] CDF and D0 Collaborations, Phys. Rev. Lett. **104**, 061802 (2010) arXiv:1001.4162 [hep-ex]
- [68] CDF and D0 Collaborations (2010 b) arXiv:1007.4587 [hep-ex]
- [69] CDF and D0 Collaborations (2011) arXiv:1107.5518 [hep-ex]
- [70] GFitter collaboration, M. Baak, *et al.*, Eur.Phys.J. C **72** 2003 (2012) arXiv:1107.0975 [hep-ph]
- [71] M. L. Mangano, M. Moretti, F. Piccinini and M. Trecani, JHEP **0701**, 013 (2007) arXiv:hep-ph/0611129
- [72] J. Alwall *et al.*, JHEP **1106**, 128 (2011) arXiv:hep-ph/1106.0522
- [73] P. Nason, JHEP **0411** 040 (2004) hep-ph/0409146
- [74] S. Frixione, P. Nason and C. Oleari, JHEP **0711**, 070 (2007) arXiv:0709.2092
- [75] S. Alioli, P. Nason, C. Oleari and E. Re, JHEP **1006**, 043 (2010) arXiv:1002.2581
- [76] T. Sjöstrand, S. Mrenna, and P. Skand, JHEP **0605**, 026 (2006) arXiv:hep-ph/0603175
- [77] CDF Collaboration, Phys. Rev. Lett. **103**, 092002 (2009) arXiv:0903.0885 [hep-ex]
- [78] D0 Collaboration, Phys. Rev. Lett. **103**, 092001 (2009) arXiv:0903.0850 [hep-ex]
- [79] E. Boos, V. Bunichev, M. Dubinin, L. Dudko, V. Ilyin, A. Kryukov, V. Edneral, V. Savrin, A. Semenov, and A. Sherstnev, Nucl. Instrum. Methods Phys. Res., Sect. A **534**, 250 (2004)
- [80] E. E. Boos, V. E. Bunichev, L. V. Dudko, V. I. Savrin, and A. V. Sherstnev, Phys. Atom. Nucl. **69**, 1317 (2006).
- [81] S. Frixione and B.R. Webber, J. High Energy Phys. **06** 029 (2002).
- [82] T. Binoth *et al.*, JHEP **0612**, 046 (2006) arXiv:hep-ph/0611170
- [83] T. Binoth, N. Kauer, P. Mertsch (2008) arXiv:hep-ph/0807.0024
- [84] CDF Collaboration, J. Phys. G **34**, 2457 (2007) arXiv:hep-ex/0508029
- [85] D0 Collaboration, Nucl. Instrum. Methods, Phys. Res. A **565**, 463 (2006) arXiv:physics/0507191
- [86] For a recent review, see P. C. Bhat, Ann. Rev. Nucl. Part. Sci. **61**, 281 (2011). The specific details of the MVA for each analysis are described in the respective references.
- [87] D0 Collaboration, Nucl. Instrum. Methods, Phys. Res. A **620**, 490 (2010)
- [88] CDF Collaboration, Nucl.Instrum.Meth. A **697** 64 (2013) arXiv:1205.1812 [hep-ex]
- [89] CDF Collaboration, Phys. Rev. D **72**, 052003 (2005) arXiv:hep-ex/0504053
- [90] ATLAS Collaboration, JINST **03** S08003 (2008) <http://inspirehep.net/record/796888/>.
- [91] CMS Collaboration, JINST **03** S08004 (2008) [http://inspirehep.net/record/796887](http://inspirehep.net/record/796887/).
- [92] S. Baffioni *et al.*, Eur. Phys. J. C **49**, 1099 (2007) <http://inspirehep.net/record/713909>
- [93] CMS Collaboration, CMS-PAS-EGM-10-004 (2010) <http://cdsweb.cern.ch/record/1299116>.
- [94] ATLAS Collaboration, JHEP **1012**, 060 (2010) arXiv:1010.2130 [hep-ex]
- [95] CMS Collaboration, CMS-PAS-PFT-10-003 (2010 b) <http://cds.cern.ch/record/1279347>
- [96] CMS Collaboration, CMS-PAS-MUO-10-002 (2010 c) <http://cdsweb.cern.ch/record/1279140>.
- [97] CMS Collaboration, JINST **7** P01001 (2012) arXiv:1109.6034 [physics]
- [98] ATLAS Collaboration, ATLAS-CONF-2011-152 (2011) <http://cdsweb.cern.ch/record/1398195>.
- [99] ATLAS Collaboration, ATL-PHYS-PUB-2011-007 (2011 b) <http://cdsweb.cern.ch/record/1345329>.
- [100] M. Cacciari, G. P. Salam and G. Soyez, JHEP **0804**, 063 (2008) arXiv:0802.1189 [hep-ph]
- [101] CMS Collaboration, CMS-PAS-BTV-10-001 (2010 d) <http://cdsweb.cern.ch/record/1279144>.
- [102] ATLAS Collaboration, ATLAS-CONF-2011-102 (2011 c) <http://cdsweb.cern.ch/record/1369219>.
- [103] CMS Collaboration, CMS-PAS-PFT-09-001 (2009) <http://cdsweb.cern.ch/record/1194487>.
- [104] ATLAS Collaboration, Eur. Phys. J. C **72**, 1844 (2012) arXiv:1108.5602 [hep-ex]

- [105] CMS Collaboration, CMS-PAS-PFT-09-001 (2009 b) <http://cdsweb.cern.ch/record/1194487>.
- [106] CMS Collaboration, CMS-PAS-PFT-10-002 (2010 e) <http://cds.cern.ch/record/1279341>
- [107] CDF Collaboration, JHEP 1302 004 (2013 b) arXiv:1208.6445 [hep-ex]
- [108] CDF and D0 Collaborations, Phys. Rev. Lett. 109, 071804 (2012) arXiv:1203.3782 [hep-ex]
- [109] CDF Collaboration, Phys.Rev.Lett. 109, 111804 (2012) arXiv:1207.1703 [hep-ex]
- [110] D0 Collaboration, Phys.Rev.Lett. 109, 121802 (2012) arXiv:1207.6631 [hep-ex]
- [111] CDF Collaboration, Phys.Rev.Lett. 103, 101802 (2009 b) arXiv:0906.5613 [hep-ex]
- [112] D0 Collaboration, Phys. Rev. Lett. 102, 051803 (2009 b) arXiv:0808.1970 [hep-ex]
- [113] CDF Collaboration, Phys.Rev.Lett. 109, 111804 (2012 b) arXiv:1207.1703 [hep-ex]
- [114] D0 Collaboration, Phys. Rev. Lett. 109, 121804 (2012 b) arXiv:1208.0653 [hep-ex]
- [115] CDF Collaboration, Phys.Lett. B715, 98 (2012 c) arXiv:1203.5815 [hep-ex]
- [116] D0 Collaboration, Phys. Rev. Lett. 105, 251801 (2010 b) arXiv:1008.3564 [hep-ex]
- [117] CDF Collaboration, Phys.Rev.Lett. 109, 111803 (2012 d) arXiv:1207.1704 [hep-ex]
- [118] D0 Collaboration, Phys. Rev. Lett. 109, 121803 (2012 c) arXiv:1207.5819 [hep-ex]
- [119] CDF Collaboration, Phys.Rev.Lett. 104, 131801 (2010) arXiv:0911.3935 [hep-ex]
- [120] D0 Collaboration, Phys. Rev. Lett. 104, 071801 (2010 c) arXiv:0912.5285 [hep-ex]
- [121] CDF Collaboration, Phys.Rev.Lett. 109, 111805 (2012 e) arXiv:1207.1711 [hep-ex]
- [122] D0 Collaboration, Phys. Lett. B 716, 285 (2012 d) arXiv:1207.5689 [hep-ex]
- [123] CDF Collaboration, Phys. Rev. Lett. 109, 111802 (2012 f) arXiv:1207.1707 [hep-ex]
- [124] D0 Collaboration, Phys. Rev. Lett. 109, 121802 (2012 e) arXiv:1207.6631 [hep-ex]
- [125] CDF Collaboration, “Search for the standard model Higgs boson in  $\tau^+\tau^-$  plus jets final state with  $8.3 \text{ fb}^{-1}$  of CDF data”, CDF Conference Note 10625 (2011)
- [126] CDF Collaboration, “Search for the standard model Higgs in the  $l\nu\tau\tau$  and  $l\ell\tau\tau$  channels”, CDF Conference Note 10500 (2011 b)
- [127] D0 Collaboration, “Search for the standard model Higgs boson in tau pair final states”, D0 Conference note 6305 (2012 f).
- [128] D0 Collaboration, “Search for a standard model Higgs boson in the  $\tau\tau\mu$  final state with  $7.0 \text{ fb}^{-1}$  at  $\sqrt{s} = 1.96 \text{ TeV}$ ”, D0 Conference Note 6286 (2012 g).
- [129] CDF Collaboration, Phys.Lett. B717, 173 (2012 g) arXiv:1207.6386 [hep-ex]
- [130] D0 Collaboration, “Search for the Standard Model Higgs boson in  $\gamma\gamma + X$  final states at D0 with  $9.7 \text{ fb}^{-1}$  of data”, D0 Conference Note 6295 (2012 h).
- [131] CDF Collaboration, Phys.Rev.Lett. 109 181802 (2012 h) arXiv:1208.2662 [hep-ex]
- [132] CDF Collaboration, “Search for standard model Higgs boson production in association with  $t\bar{t}$  using no lepton final state”, CDF Conference Note 10582 (2011 c)
- [133] CDF Collaboration, Phys. Rev. Lett. 78, 4536 <http://inspirehep.net/record/423258/> (1997)
- [134] D0 Collaboration, Phys. Rev. Lett. 94, 151801 (2005) arXiv:hep-ex/0410066, [Erratum-ibid. 100, 139901 (2008)]
- [135] CDF Collaboration, Phys. Rev. Lett. 98, 161801 (2007 b) arXiv:hep-ex/0702027]
- [136] D0 Collaboration, Phys. Rev. Lett. 101, 171803 (2008) arXiv:0808.0703 [hep-ex]
- [137] D0 Collaboration, Phys. Rev. Lett. 103, 191801 (2009 c) arXiv:0904.0673 [hep-ex]
- [138] CDF Collaboration, Phys. Rev. Lett. 104, 201801 (2010 b) arXiv:0912.4500 [hep-ex]
- [139] CDF Collaboration, Phys. Rev. D86, 031104 (2012 i) arXiv:1202.6629 [hep-ex]
- [140] D0 Collaboration, Phys.Rev. D85, 112005 (2012 i) arXiv:1201.5652 [hep-ex]
- [141] CDF Collaboration, Phys. Rev. Lett. 108, 101801 (2012 j) arXiv:1112.2978 [hep-ex]
- [142] CDF Collaboration, Phys. Rev. Lett. 104, 101801 (2010 c) arXiv:0911.4449 [hep-ex]
- [143] D0 Collaboration, Phys. Rev. Lett. 102, 161801 (2009 d) arXiv:0810.3873 [hep-ex]
- [144] CDF Collaboration, Phys. Rev. Lett. 103, 091803 (2009 c) arXiv:0905.4714 [hep-ex]
- [145] CDF Collaboration, “Search for  $H \rightarrow WW^*$  production using  $9.7 \text{ fb}^{-1}$ ”, CDF Conference Note 10785 (2012 k)
- [146] D0 Collaboration, “Search for Higgs boson production in dilepton plus missing energy final states with  $8.6 - 9.7 \text{ fb}^{-1}$  of  $p\bar{p}$  collisions at  $\sqrt{s} = 1.96 \text{ TeV}$ ”, D0 Conference Note 6302 (2012 j).
- [147] D0 Collaboration, “Search for associated Higgs boson production with  $VH \rightarrow e^\pm\nu_e\mu^\pm\nu_\mu + X$  like charged electron muon pairs using  $9.7 \text{ fb}^{-1}$  of  $p\bar{p}$  collisions at  $\sqrt{s} = 1.96 \text{ TeV}$ ”, D0 Conference Note 6301 (2012 k).
- [148] D0 Collaboration, “Search for standard model Higgs boson with tri-leptons and missing transverse energy with  $9.7 \text{ fb}^{-1}$  of  $p\bar{p}$  collisions at  $\sqrt{s} = 1.96 \text{ TeV}$ ”, D0 Conference Note 6276 (2012 l).
- [149] D0 Collaboration, Phys. Rev. Lett. 106, 171802 (2011) arXiv:1001.6079v2 [hep-ph]
- [150] CDF Collaboration, “Search for  $H \rightarrow WW^*$  with leptons and hadronic taus in the final state using  $9.7 \text{ fb}^{-1}$ ”, CDF Conference Note 10781 (2012 l)
- [151] CDF Collaboration, Phys.Rev. D86 072012 (2012 m) arXiv:1207.5016 [hep-ex]
- [152] C. Anastasiou, G. Dissertori, M. Grazzini, F. Stockli and B. R. Webber, JHEP 0908, 099 (2009 b) arXiv:0905.3529 [hep-ph]
- [153] J. M. Campbell, R. K. Ellis and C. Williams, (2010) arXiv:1005.3733 [hep-ph].
- [154] CDF Collaboration, CDF Note 10804 (2012 n) [www-cdf.fnal.gov/physics/new/hdg/Results\\_files/results/cdfcomb\\_mar2012/](http://www-cdf.fnal.gov/physics/new/hdg/Results_files/results/cdfcomb_mar2012/)
- [155] D0 Collaboration, D0 Note 6304-CONF (2012 m) [www-d0.fnal.gov/Run2Physics/WWW/results/prelim/HIGGS/H128/](http://www-d0.fnal.gov/Run2Physics/WWW/results/prelim/HIGGS/H128/)
- [156] CMS Collaboration, JHEP 1201, 133 (2012 b) arXiv:1110.6461 [hep-ex]
- [157] ATLAS Collaboration, Phys. Rev. Lett. 107, 041802 (2011 d) arXiv:1104.5225 [hep-ex]
- [158] CMS Collaboration, Phys. Lett. B 699, 25 (2011) arXiv:1102.5429 [hep-ex]
- [159] ATLAS Collaboration, Phys. Lett. B 712, 289 (2012 b) arXiv:1203.6232 [hep-ex]
- [160] ATLAS Collaboration, ATLAS-CONF-2012-025 (2012)



- c)  
<http://cdsweb.cern.ch/record/1430734>.
- [161] CMS Collaboration, CMS-PAS-SMP-12-005 (2012 c)  
<http://cdsweb.cern.ch/record/1440234>.
- [162] CMS Collaboration, CMS-PAS-SMP-12-013 (2012 d)  
<http://cdsweb.cern.ch/record/1460099>.
- [163] ATLAS Collaboration, Phys. Rev. Lett. 108, 041804 (2012 d) arXiv:1110.5016 [hep-ex]
- [164] CMS Collaboration, JHEP 01 063 (2013) arXiv:1211.4890 [hep-ex]
- [165] ATLAS Collaboration, ATLAS-CONF-2012-090 (2012 e)  
<http://cdsweb.cern.ch/record/1460409>
- [166] CMS Collaboration, Submitted to Phys. Lett. B (2013 b) arXiv:1301.4698 [hep-ex]
- [167] ATLAS Collaboration, Phys. Rev. Lett. 108, 111803 (2012 f) arXiv:1202.1414 [hep-ex]
- [168] ATLAS Collaboration, ATLAS-CONF-2012-091 (2012 g)  
<http://cds.cern.ch/record/1460410>
- [169] CMS Collaboration, Phys. Lett. B 710, 403 (2012 e) arXiv:1202.1487 [hep-ex]
- [170] CMS Collaboration, CMS-PAS-HIG-12-015 (2012 f)  
<http://cdsweb.cern.ch/record/1460419>.
- [171] ATLAS Collaboration, Phys. Lett. B 710, 383 (2012 h) arXiv:1202.1415 [hep-ex]
- [172] ATLAS Collaboration, ATLAS-CONF-2012-092 (2012 i)  
<http://cdsweb.cern.ch/record/1460411>.
- [173] CMS Collaboration, Phys.Rev.Lett. 108, 111804 (2012 g) arXiv:1202.1997 [hep-ex]
- [174] CMS Collaboration, CMS-PAS-HIG-12-016 (2012 h)  
<http://cdsweb.cern.ch/record/1460664>.
- [175] CMS Collaboration, JHEP 1203, 081 (2012 i) arXiv:1202.3617 [hep-ex]
- [176] CMS Collaboration, CMS-PAS-SMP-12-009 (2012 j)  
<http://cdsweb.cern.ch/record/1431862>.
- [177] ATLAS Collaboration, Phys. Lett. B, 716, 62 (2012 j) arXiv:1206.0756 [hep-ex]
- [178] ATLAS Collaboration, ATLAS-CONF-2012-098 (2012 k)  
<http://cdsweb.cern.ch/record/1462530>.
- [179] CMS Collaboration, CMS-PAS-HIG-12-017 (2012 k)  
<http://cdsweb.cern.ch/record/1460424>.
- [180] CMS Collaboration, Phys. Lett. B 710, 91 (2012 l) arXiv:1202.1489 [hep-ex]
- [181] ATLAS Collaboration, Phys.Lett. B718, 391 (2012 l) arXiv:1206.6074 [hep-ex].
- [182] CMS Collaboration, CMS-HIG-12-003 (2012 m)  
<http://cds.cern.ch/record/1449158>
- [183] CMS Collaboration, CMS-HIG-12-021 (2012 n)  
<http://cdsweb.cern.ch/record/1460660>
- [184] ATLAS Collaboration, Phys.Lett. B717, 70 (2012 m) arXiv:1206.2443 [hep-ex].
- [185] CMS Collaboration, JHEP 1204, 036 (2012 o) arXiv:1202.1416 [hep-ex]
- [186] ATLAS Collaboration, Phys.Lett. B717, 29 (2012 n) arXiv:1205.6744 [hep-ex]
- [187] CMS Collaboration, JHEP 1203, 040 (2012 p) arXiv:1202.3478 [hep-ex]
- [188] CMS Collaboration, CMS-PAS-HIG-12-023 (2012 q)  
<http://cdsweb.cern.ch/record/1460693>.
- [189] ATLAS Collaboration, JHEP 1209, 070 (2012 o) arXiv:1206.5971 [hep-ex]
- [190] CMS Collaboration, Phys. Lett. B 713, 68 (2012 r) arXiv:1202.4083 [hep-ex]
- [191] CMS Collaboration, CMS-PAS-HIG-12-018 (2012 s)  
<http://cdsweb.cern.ch/record/1460413>.
- [192] ATLAS Collaboration, Phys.Lett. B718, 369 (2012 p) arXiv:1207.0210 [hep-ex]
- [193] CMS Collaboration, Phys. Lett. B 710, 284 (2012 t) arXiv:1202.4195 [hep-ex]
- [194] CMS Collaboration, CMS-PAS-HIG-12-019 (2012 u)  
<http://cdsweb.cern.ch/record/1460692>.
- [195] ATLAS Collaboration, ATLAS-CONF-2012-135 (2012 q)  
<http://cdsweb.cern.ch/record/1478423>.
- [196] CMS Collaboration, CMS-PAS-HIG-12-020 (2012 v)  
<http://cdsweb.cern.ch/record/1460438>.
- [197] ATLAS Collaboration, ATLAS-CONF-2012-019 (2012 r)  
<http://cds.cern.ch/record/1430033>
- [198] ATLAS Collaboration, Phys. Lett. B 710, 49 (2012 s) arXiv:1202.1408 [hep-ex]
- [199] ATLAS Collaboration, Phys. Lett. B 716, 1 (2012 t) arXiv:1207.7214 [hep-ex]
- [200] CMS Collaboration, Phys. Lett. B 710, 26 (2012 w) arXiv:1202.1488 [hep-ex]
- [201] CMS Collaboration, Phys. Lett. B 716, 30 (2012 x) arXiv:1207.7235 [hep-ex]
- [202] ATLAS Collaboration, ATLAS-CONF-2012-127 (2012 u)  
<http://cds.cern.ch/record/1476765>
- [203] CDF Collaboration, “Combination of CDF standard model Higgs boson searches with up to to 9.7 fb<sup>-1</sup> of data”, CDF Conference Note 10804 (2012 o)
- [204] D0 Collaboration, “Combined Upper Limits on Standard Model Higgs Boson Production from the D0 Experiment in up to 9.7 fb<sup>-1</sup> of data”, D0 Conference Note 6304 (2012 n)